Journal of Water Process Engineering 44 (2021) 102354

Contents lists available at ScienceDirect

Journal of Water Process Engineering

journal homepage: www.elsevier.com/locate/jwpe

Novel insights into the nanoadsorption mechanisms of crystal violet using nano-hazelnut shell from aqueous solution

Mashael A. Al-Ajji, Mohammad A. Al-Ghouti *

Environmental Science Program, Department of Biological and Environmental Sciences, College of Arts and Sciences, Qatar University, State of Qatar – Doha. P.O. Box: 2713

ARTICLE INFO

Keywords:
Nanoadsorption
Low-cost agricultural waste
Crystal violet dye
Biosorption
Adsorption process

ABSTRACT

This paper discusses the nanoadsorption mechanisms of crystal violet (CV) using a nano-hazelnut shell (nano-HS) from an aqueous solution. The effect of various factors such as pH, temperature, and initial CV concentration on the adsorption process was also evaluated. The physical and chemical characterizations of hazelnut shells (HS) and nano-HS were studied using Fourier transform infrared spectroscopy (FTIR), scanning electron microscopy (SEM), and transmission electron microscope (TEM). Various functional groups including —OH, C═O, C—H, and C—O were identified that are facilitated the CV sorption onto the adsorbents. Additionally, the SEM revealed the adsorbents as a heterogeneous structure with deep cavities and high porosity, which is thought to play a vital role in capturing and binding the CV ions onto the surface of the adsorbent. The optimum pH in this study was reported to be 10. While Langmuir isotherm was identified as the best-suited model to describe the adsorption process, with a 93% and 96% correlation coefficient for HS and nano-HS, respectively. 181.82 mg/g was the maximum adsorption capacity for HS and 294.12 mg/g for nano-HS at 45 °C. Additionally, the positive value of changes in enthalpy for HS (21.912 kJ/mol) indicated the reaction was endothermic while the negative value (−47.541 kJ/mol) for nano-HS signifies that the CV adsorption onto was an exothermic reaction. The Gibbs free energy was found to increase with smaller nanoparticle sizes. On the other hand, the effects of particle size on the enthalpy and the entropy were increased.

1. Introduction

Water pollution has increased exponentially with the increase in the human population as such textile industry is considered one of the major industries that consume a high quantity of chemicals and water and as a result, produces environmentally hazardous wastewater [1]. The use of dyes in recent years has increased exponentially. According to Ben ManSour et al. [2] around 800,000 tons of dyes are produced every year. Cationic dyes are most commonly used due to their high solubility and ease of dyeing various fabrics including silk, wool, paper and, acrylic [3]. Due to the excess use of such products, the water discharged from the industry consists of various hazardous chemicals including heavy metals, azodyes, bisphenol A (BPA), suspended solids, high chemical oxygen demand (COD), and biological oxygen demand (BOD) [4]. Dyes cannot undergo degradation; hence, are present in water bodies for a very long time, which can prevent the passage of light into the water. This has become one of the most crucial environmental issues. Such hindrance can affect photosynthetic activities, which can affect the water quality and leads to gas solubility, and also affect the aquatic life and the food web [5]. The maximum discharge limits and toxicological effects of most dyes on the environment and human health are not yet established. However, the color limit and measurement are only required as specific limits for dyes and colored water limits. However, the typical characteristic of textile effluent is 50–2500 Pt-Co unit, and the effluent color limitation is 100 Pt-Co unit [5,6].

As such, one of the members of the triphenylmethane class of dyes is crystal violet (CV). CV is cationic and is readily used in textile, paper, and other fields and subsequently found in wastewater effluent. CV is considered carcinogenic hazardous, and mutagenic for living organisms and categorized as a rebellious molecule that is non-biodegradable hence persists in the environment for a very long time [7]. In addition, it is known to be detrimental for both aquatic animals and humans. For aquatic animals it is known to be responsible for mitotic poisoning, which is associated with the abnormal accumulation of metaphases, tumors in fishes as well as hepatocarcinoma, reticular cell sarcoma in various organs including the ovary, bladder and, uterus [8]. While in humans, it can cause chemical cystitis, irritation of the skin and

* Corresponding author.
E-mail address: mohammad.alghouti@qu.edu.qa (M.A. Al-Ghouti).

https://doi.org/10.1016/j.jwpe.2021.102354
Received 4 July 2021; Received in revised form 27 September 2021; Accepted 27 September 2021

Nomenclature

Adsorbent mass m
Brunauer-Emmett-Teller BET
Bisphenol A BPA
Biological oxygen demand BOD
Celsius °C
Chemical oxygen demand COD
Crystal violet CV
Dubinin-Radushkevich isotherm constant ε
Entropy change ΔS°
Enthalpy change ΔH°
Electrostatic potentials ESP
Freundlich constant K_F
Final concentration (after adsorption) C_e
Fourier transform infrared spectroscopy FTIR
Gibb's free energy change ΔG°
Highest occupied molecular orbital HOMO
Hydrochloric acid HCl
Hazelnut shells HS
HS nanoparticles Nano-HS
Initial concentration (before adsorption) C_0
Lowest unoccupied molecular orbital LUMO
Maximum monolayer coverage capacity Qo
Mass M
Temkin isotherm constant b_T
Toluidine Blue TB
Theoretical isotherm saturation capacity (mg/g) q_s
Temkin isotherm equilibrium binding constant A_T
The adsorption capacity Q_e
Transmission Electron Microscopy TEM
Ratio r
Scanning Electron Microscopy SEM
Sodium hydroxide NaOH

digestive tracts, respiratory and renal failure [9].

Therefore, appropriate methods to eliminate these pollutants from water are necessary before releasing them into the environment [10]. Wastewater treatment can be classified into three major groups (i) physical treatment (ii) biological treatment and (iii) chemical treatment. Fig. 1 illustrates some of their methods and the advantages and disadvantages associated with them. Although existing technologies such as membrane processes, chemical reactions, sedimentation, biological process, precipitation, electrochemical, ion exchange, coagulation-flocculation, and flotation may be efficient for removing CV from wastewater, they are rather expensive and time-consuming [11]. While electrochemical degradation and nanofiltration have not been identified as optimum solutions [12–14]. Adsorption, on the other hand, has emerged as a promising technique for treating aqueous effluent owing to its simplicity and cost-effectiveness. Over the years there have been several studies enriched with adsorption techniques for cationic dye removal from the liquid solution. Such vast studies have shown agricultural-based adsorbents as a promising alternative to the current conventional materials that are readily used [15–17]. Additionally, in recent years emerging technology incorporates nanoparticle-based adsorbents. Several researchers have investigated the adsorption of dyes using various agricultural waste including Shoukat et al. [18] used mango stone for CV removal and found adsorption capacity as 52.6 mg/g. Nguyen et al. [19] investigated the efficient removal of toxic organic dyes using a zirconium-organic framework as a recyclable nano-adsorbent. Methylene blue and methyl orange were chosen as model dye pollutants. It had a superior maximum capacity (746 mg/g and 726 mg/g, respectively) and reusability over several cycles of the adsorption. Raza et al. [20] studied the adsorption of organic dyes using a 2D copper (II)-carboxylate framework. Three organic dyes, namely methylene blue, methyl orange, and methyl red were studied. The dye removal efficiency was attributed to the shapes, synergy among structure, dimensions, and ionic strength of dyes to the adsorbent structure.

On the other hand, Moharrami & Motamedi [21] prepared cellulose nanocrystals from agricultural waste and obtained 2500 mg/g and 1428.6 mg/g adsorption capacity for CV and methylene blue, respectively. Similarly, other studies include potatoes plant waste [22], date palm leaves [23], agro-industrial [24], peanut hull waste biomass [25],

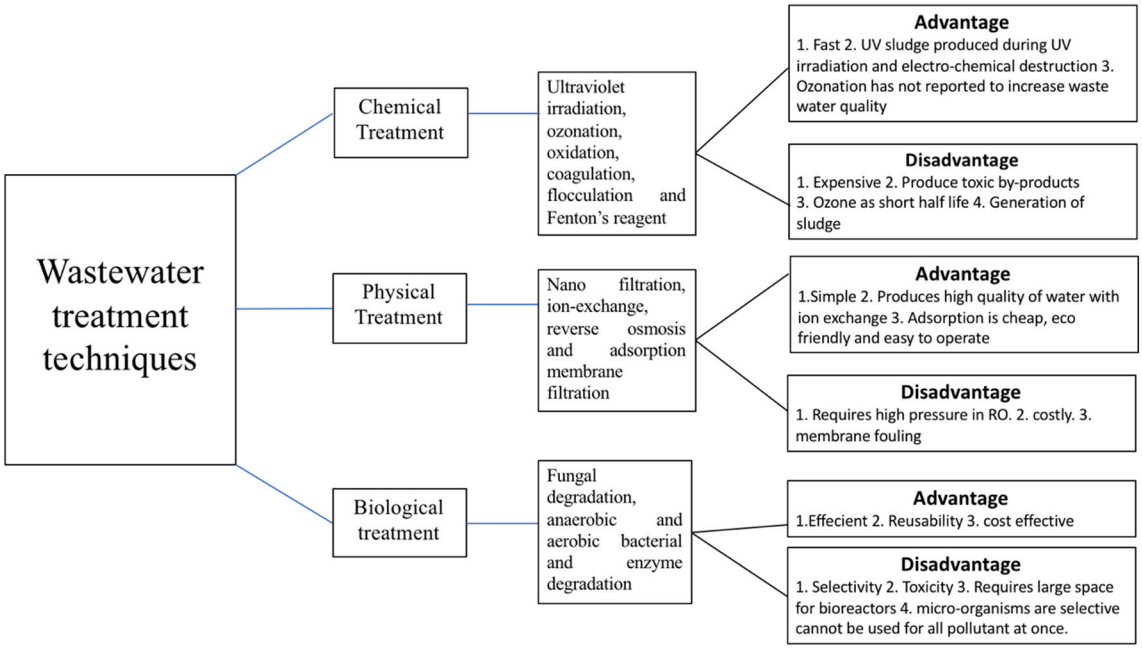

Fig. 1. Various wastewater treatment and their advantages and disadvantages [11].

sugarcane bagasse soot [26], and hyacinth [27]. While Putri et al. [28] have reported successful removal of cationic dyes from aqueous solution as well as effluents. In addition to being low-cost, such materials also inherent other advantages including minimization of waste yet delivering high efficiency in dilute solution, no additional requirement of nutrient, ease of operation, and non-hazardous to the environment [29].

Cellulose is one of the key molecules that are found in various agricultural by-products, which has been reported to be useful in the adsorption process. Cellulosic biomaterials are suitable adsorbents due to their richness in organic functional groups such as carbonyl, amine, hydroxyl, carboxyl, ester, amide, and others [30,31]. Cellulosic biomass is a heterogeneous substance that consists of cellulose, hemicellulose, and lignin as well as a complex polymer of phenylpropane units [32]. Generally, the biosorption capacity of biosorbents depends on several parameters including the physicochemical properties of the biosorbent, the presence of other competing ions, and various factors such as temperature and pH. Hazelnut shells (HS) exist in large quantities around to world as food waste. HS consists of various polar functions including alcoholic, carboxylic, and carboxylic, which can facilitate sorbent and pollutant binding [33]. Additionally, HS is beneficial because of its microporous and mesoporous structure and large surface area. Just like other agricultural waste, HS is also rich in lignin, cellulose, and hemicellulose. Various literature including Uyan et al. [34], Senol [35], and Hosgün et al. [36], Demirkaya et al. [37], and Gozaydin & Yuksel [38], studied the chemical morphology of HS. All studies found lignin as a dominant polymer present in HS, while cellulose and hemicellulose percentages varied according to region. Moreover, HS can be used in a broader context and remove other cationic dyes from an aqueous medium. Various studies were conducted to understand the adsorption mechanism of cationic dyes by HS [39–43].

Nanoparticles have widely been used as adsorbents for water and wastewater matrices, and have unique adsorption properties compared with corresponding bulk particles [13,44–47]. The effect of nanoparticle size is not well understood. Hence, it is vital to investigate the effect of nanoparticle size on the overall nanoadsorption processes and thermodynamics.

Based on our knowledge no study has investigated the removal of CV by nanoparticles of hazelnut shells. Keeping the efficiency and importance of biosorption, the present study aims to assess the efficiency and the potential of using a nano-hazelnut shell (nano-HS) for CV adsorption. The effects of pH, temperature, initial CV concentration, and particle size on the CV adsorption mechanisms onto HS and nano-HS were carried out. Additionally, the experimental data were modeled in four different isotherms, namely Langmuir, Freundlich, Dubinin-Radushkevich, and Temkin. Over and above, the effect of nanoparticle size on the adsorption thermodynamics was investigated.

2. Methodology

2.1. Materials collection and preparation hazelnut shells (HS) and HS nanoparticles (nano-HS)

Hazelnut shells were collected from a local Qatari Market. The shells were cracked, compressed, and sieved using a mechanical sieve (Retsch, 5657 HAAN W Germany) to obtain different particle size ranges. Each particle size range was collected, stored in a glass bottle, and kept in a dry place. The (0.125 mm–0.250 mm) range was used throughout the HS experiments. The HS nanoparticles (nano-HS) were attained from CryoMill (Retsch CryoMill). The nano-HS were washed with distilled water three times and dried in the oven overnight at 65 °C.

2.2. Preparation of stock solution of crystal violet

A stock solution of 1000 mg/L of CV was prepared in distilled water. The CV was obtained from Breckland Scientific Supplies Ltd. (chemical formula $C_{25}H_{30}N_3Cl$, molecular weight 407.98 g/mol, $\lambda_{max} = 591$ nm).

2.3. Characterization of the adsorbents (HS and nano-HS)

Physical and chemical characterizations of HS and nano-HS were studied. Scanning electron microscopy (SEM) (Nova™ Nano SEM 50 Series) and transmission electron microscope (TEM) were used to determine the surface characterization and understand the morphology of the adsorbent. Brunauer– Emmett–Teller (BET) (Quantachrome Corporation, Nova 3000) was used to determine the surface areas and pore size distribution. Fourier transform infrared spectroscopy using a universal attenuated total reflectance sensor (FTIR-UATR) (PerkinElmer, spectrum range: 400 cm^{-1} to 4000 cm^{-1}) was used to determine the functional group present on the surface of the adsorbents.

2.4. The effect of pH on the adsorption capacity of CV onto HS and nano-HS

The adsorption experiment for the effect of pH was carried out at different pH (2, 4, 6, 8, and 10). The diverse pH values of CV solution were adjusted by adding 0.1 M sodium hydroxide (NaOH) and 0.1 M hydrochloric acid (HCl) solution using a pH meter (pH meter, Jenway 370). A mass of 0.05 g of the adsorbent was added to the glass beaker. Subsequently, the samples were kept in the rotary shaker (Brunswick Innova® 2100/2150 Shaker) at 160 rpm for 48 h (the defined adsorption equilibrium time) at room temperature. Then, the bottles were removed, filtrated, and analyzed using a UV–Vis spectrometer (PerkinElmer Lambda 25 UV/Vis). The experiments were performed in triplicate and the average values were used to demonstrate the results.

2.5. Effect of initial concentration and solution temperature on the adsorption capacity of CV onto HS and nano-HS

The batch adsorption experiments were carried out at different initial CV concentrations, (20 mg/L, 50 mg/L, 100 mg/L, 200 mg/L, 300 mg/L, 400 mg/L, 500 mg/L, 700 mg/L, 800 mg/L, and 1000 mg/L). The mass (m) to volume (V) ratio (m:V) was kept as 1:1. 0.05 g of the adsorbent was added in the borosilicate glass bottles and the final volume was adjusted to 50 mL. Based on the pH batch adsorption experiment (Section 2.4) results, the CV solution was adjusted to pH 10 for both adsorbents. The bottles were placed in a rotary shaker (Brunswick Innova® 2100/2150 Shaker) at 25 °C for 48 h at 160 rpm.

To determine the effect of temperature on the adsorption process, the batch CV adsorption experiments were conducted at different solution temperatures, 25 °C, 35 °C, and 45 °C. The same protocol was followed for HS. To validate the data, the experiments were performed in triplicates and average values were presented,

The solution was then filtered using a syringe and a 0.20-μm membrane filter, and the nano-HS size was filtered by first centrifuging (Heraeus™ Megafuge™ 16 Centrifuge Series) and then carrying out filtration. The separated solutions were diluted prior to UV–Vis spectrophotometer analysis. The adsorption capacity (Q_e, mg/g) was calculated by Eq. (1) [48],

$$Q_e = \frac{(C_0 - C_e) \times V}{m} \times 100\% \quad (1)$$

where C_0 and C_e are the initial and equilibrium CV concentration (mg/L) before and after adsorption, receptively, V is the CV solution volume (L) and m is the adsorbent mass (g).

2.6. Adsorption isotherm

Table 1 shows the four isotherm models that were studied in the current study.

Table 1
Four isotherm models used in the study.

Isotherm model	Linear form	Non-linear form	Plot	Parameters
Langmuir	$\frac{C_e}{q_e} = Q_\circ - \frac{q_e}{bC_e}$	$q_e = \frac{Q_\circ bC_e}{1+bC_e}$	$\frac{C_e}{q_e}$ $Vs{\cdot}Q_\circ$	Ce: Equilibrium concentration of adsorbate on the adsorbent (mg/L); b: Langmuir isotherm constant or affinity constant (dm^3/mg); qe: Amount of the adsorbate at equilibrium (mg/g); Q_o: Maximum monolayer coverage capacity (mg/g); A_T: Temkin isotherm equilibrium binding constant in (L/g); b_T: Temkin isotherm constant which is related to sorption heat (J/mol); K_F: Freundlich constant ((mg/g)/(g/L)$^{1/n}$); $1/n$: the intensity of the adsorption or surface heterogeneity indicating the energy relative distribution and the adsorbate sites' heterogeneity; q_s: Theoretical isotherm saturation capacity (mg/g) ε: Dubinin–Radushkevich isotherm constant [49]
Freundlich	$logq_e = logK_F + \frac{1}{n}logC_e$	$q_e = K_F C_e \frac{1}{n}$	$logq_e Vs \cdot logC_e$	
Dubinin-Radushkevich	$lnq_e = q_s - K\varepsilon^2$	$q_e = q_s e^{-K\varepsilon 2}$	lnq_e $Vs \cdot \varepsilon^2$	
Temkin	$q_e = \frac{RT}{b_T} lnA_T + \left(\frac{RT}{b_T}\right) lnC_e$	$q_e = \frac{RT}{b_T} ln A_T C_e$	q_e $Vs.\cdot$ ln C_e	

2.7. Thermodynamic studies

The thermodynamics was studied by determining various parameters including entropy change (ΔS°), enthalpy change (ΔH°), and Gibb's free energy change (ΔG°) using Eqs. (2), (3) and (4) [50],

$$lnK_e = -\frac{\Delta H^o}{RT} + \frac{\Delta S^O}{R} \quad (2)$$

$$\Delta G^o = -\mathrm{RTLn}\,(K_c) \quad (3)$$

$$\Delta G^o = \Delta H^o - T\Delta S^o \quad (4)$$

2.8. Statistical analysis

The significant difference between the means of samples was determined using Microsoft excel double factor two-way ANOVA. Furthermore, it also helped to understand if there is any interaction between the two variables (independent and dependent).

3. Result and discussion

3.1. FTIR characterization

Fig. 2 shows the FTIR spectra of HS and nano-HS before and after the CV adsorption. The peak at 3320 cm^{-1} belongs to the —OH functional group, which is a common macromolecule found on cellulose, lignin, and hemicellulose [17,34,51]. Another possible explanation can also be the presence of water molecules [52]. The peak at 2921 cm^{-1} in Fig. 2B is shifted to 2892 cm^{-1} after adsorption, whichshowed the presence of C—H stretch [19,53]. The peaks are shown at 1735 cm^{-1} and 1731 cm^{-1}

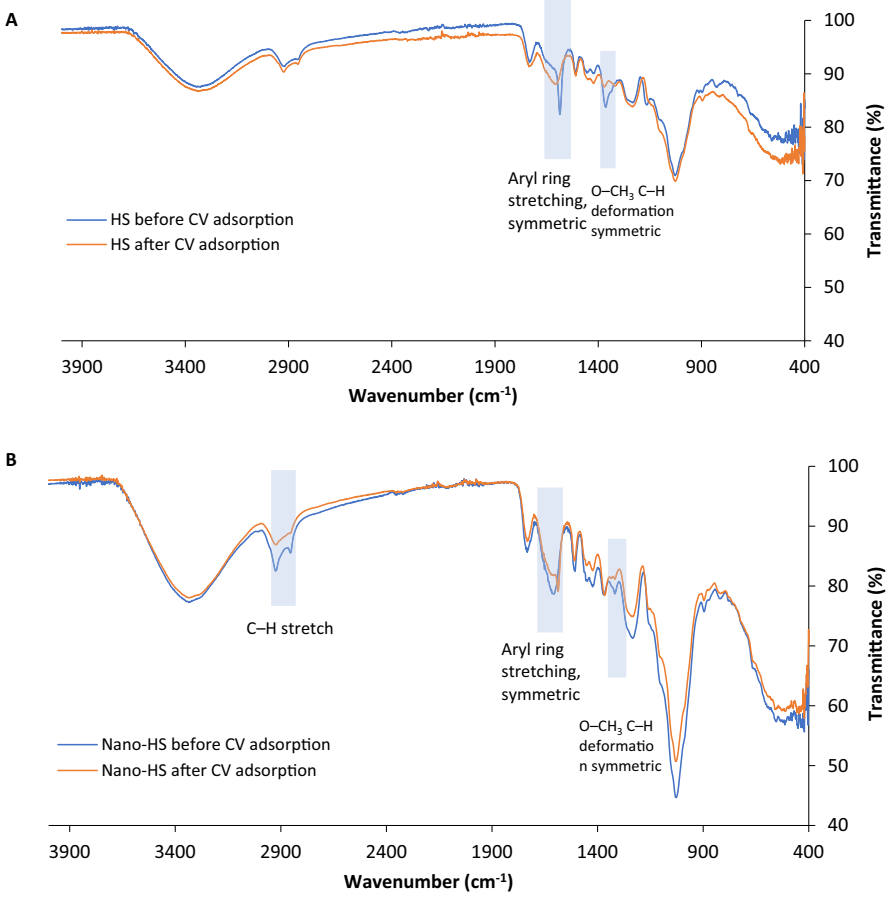

Fig. 2. FTIR spectra of (A) HS and (B) nano-HS before and after the CV adsorption.

in Fig. 2A and 2B, respectively; suggesting the presence of the carboxylic acid group in hemicellulose [30,54]. The bands around 1650 cm^{-1} and 1750 cm^{-1} in both Fig. 2A and 2B marked the presence of free esterified carboxyl groups. While, the bands at 1584 cm^{-1} and 1587 cm^{-1} in Fig. 2A and 2B, respectively; attributing to the CO stretch of the carboxyl group of C═O [55,56]. A strong sharp peak that was observed at 1024 cm^{-1} and 1014 cm^{-1} further confirmed the presence of cellulose in HS [55]. Lastly, the presence of a peak in 1030 cm^{-1}–1046 cm^{-1} was assigned to the C—O of alcohol and carboxylic acids [56]. The FTIR spectra indicated that the HS adsorbent in general consists of various carbons forms including aliphatic, aromatic, and cyclic as observed from the various peaks. Additionally, it also demonstrates that HS in general has a heterogeneous surface with various functional groups present that will aid the adsorption of crystal violet ions. Furthermore, the presence of such functional groups on the hazelnut shells including alcoholic, carbonylic, carboxylic, and phenolic facilitated the adsorption rate by further increasing the negative charge leading to the high adsorption capacity of HS at high pH [57]. Fig. 3 illustrates the major functional groups and the corresponding peaks that were reported for lignin, hemicellulose, and cellulose [44,58,59]. The main composition of the three materials (i.e. cellulose, hemicellulose, and lignin) is alkanes, esters, aromatics, ketones, and alcohol with various oxygen-containing functional groups. It can be observed in Fig. 3 that there were two main absorbance regions approximately at low wavelengths (700 cm^{-1} - 1800 cm^{-1}) and high wavelengths (2800 cm^{-1}–3500 cm^{-1}). The peak in the range of 1500 cm^{-1} to 1600 cm^{-1} corresponds to the aromatic ring vibrations, which confirms the presence of lignin. The absorbance around the 1730 cm^{-1} region could be attributed to the presence of methoxyl—O—CH_3, aromatic C═C, and C—O—C functional groups [58].

3.2. Scanning Electron Microscopy (SEM)

When comparing the surface pattern and porous forms of Fig. 4A and 4B, it is apparent that HS appeared as a porous structure. Additionally, irregular voids and pores were also shown. In general, both adsorbents appeared as irregular, rough, and mound surfaces. Moreover, several layers of fibers that merged to form spirals are attributed to cellulose structure [60]. These spiral-like structures are expected to capture CV ions on the surface. Additionally, the irregular and rough structures are evident for nano-HS as seen in Fig. 4C and 4D. These irregular morphologies are expected to facilitate the binding of CV onto the adsorbent while preventing desorption [61]. It is evident that both adsorbents vary with their morphologies and have vivid different structures. However, nano-HS is more heterogeneous and consists of a much rougher surface as oppose to HS this specific characteristic is expected to increase the chances of adsorption. Additionally, the BET analysis revealed that nano-HS has a larger surface area, which is 4.885 m^2/g, and a high pore radius size of 76.3 nm, while HS surface area was 3.709 m^2/g, and pore radius size was 50.6 nm. These characteristics indeed will play an important role in the CV ions adsorption [62,63]. Additionally, The EDX data revealed that the particles had a high concentration of carbon (73%) followed by oxygen (21.0%) as shown in Fig. 5D.

The different regions of CV accumulation can be visualized from Fig. 4E–4H. The successful capture of CV onto HS can be seen in Fig. 4E and 4F, where the high porosity and deep cavities helped capture CV ions on the surface. Additionally, as observed from SEM and FTIR, HS, in general, consists of various functions that facilitated the binding of CV onto HS. The intraparticle diffusion as observed in Fig. 4G and 4H occurred because of the effective pore volume diffusion. Generally, the surface diffusion was insignificant owing to the intricate structure of the adsorbent.

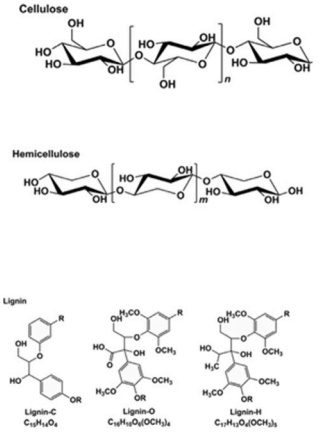

HS (cm^{-1})		Nano-HS (cm^{-1})		Assignment
3331	s,b	3331	vs,b	O–H stretch, H-bonded
2924	w	2924	m	C–H stretch methyl and methylene groups
2863	sh	2863	w	C–H stretch in methyl and methylene groups
1729	sh	1737	m	C-O stretch, unconjugated ketone, carboxyl, and ester groups
1584	m	1609	s	Aryl ring stretching, symmetric
1511	m	1511	m	Aryl ring stretch, asymmetric
1456	sh	1456	sh	O–CH_3 C–H deformation, asymmetric
1426	sh	1426	sh	Aromatic skeletal vibration combined with C–H in plane deformation
1371	w	1371	sh	O–CH_3 C–H deformation symmetric
1315	sh	1315	sh	Aryl ring breathing with C–O stretch
1235	m	1228	s	Aryl ring breathing with C–O stretch
1151	sh	1139	sh	Aromatic C–H in plane deformation
1084	sh	1098	sh	C–O deformation, secondary alcohol, and aliphatic ether
1024	s	1027	vs	Aromatic C–H in plane deformation
891	vw	891	vw	C–H deformation of out of plane, aromatic ring
809	vw	891	vw	C–H deformation of out of plane, aromatic ring

b: broad, vs: very strong; s: strong; m: medium; w: weak; vw: very weak; sh: shoulder; relative to other peaks in the spectrum.

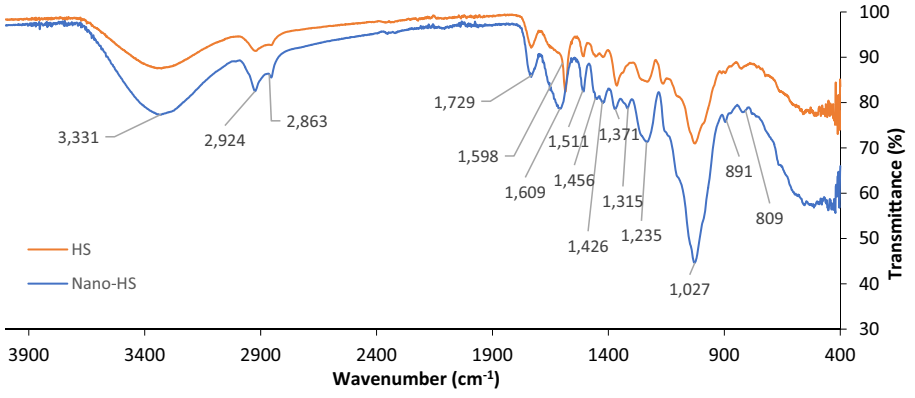

Fig. 3. Absorption peaks for major functional groups of cellulose, hemicellulose, and lignin [44,58,59].

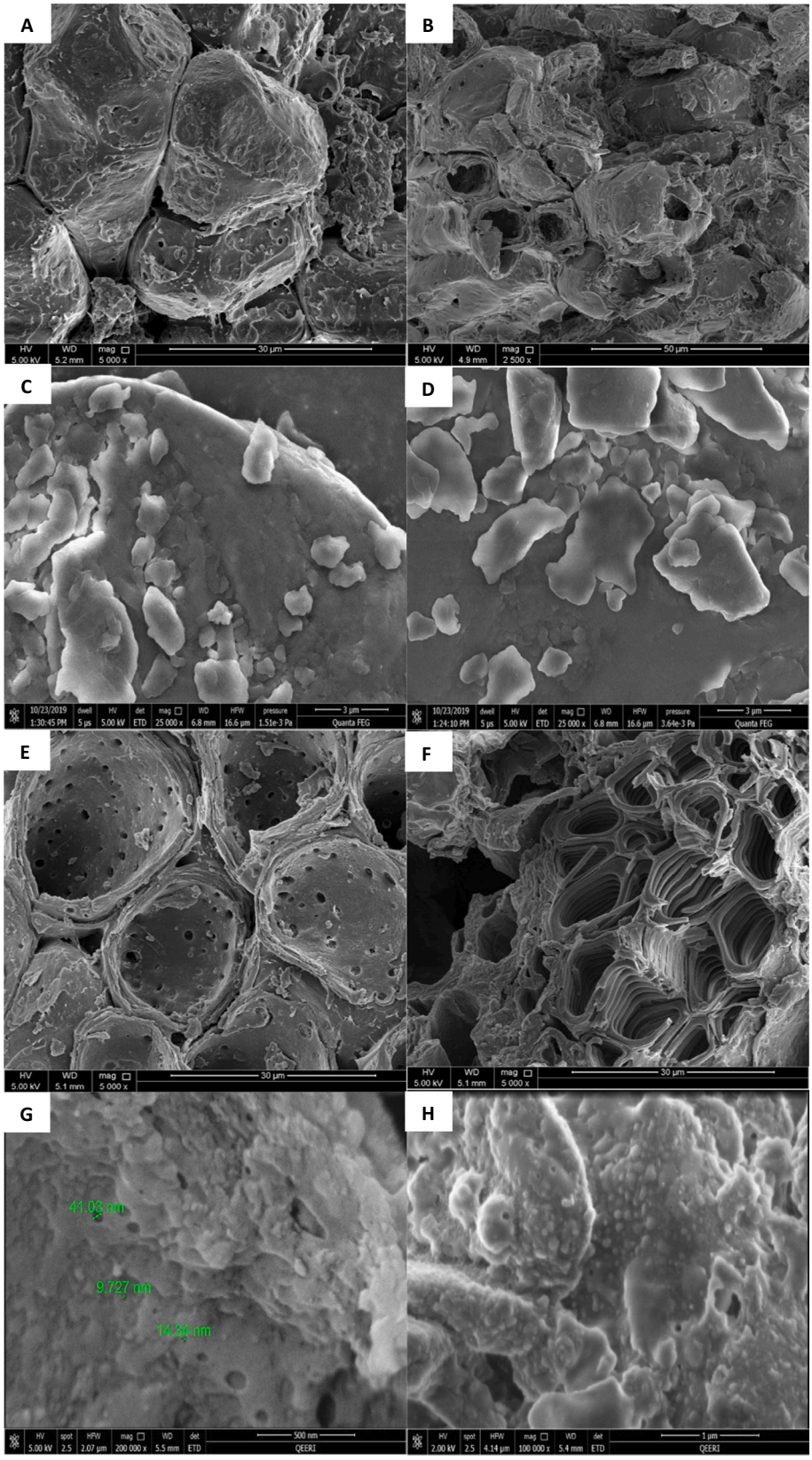

Fig. 4. SEM images of HS (A) ×5000 and (B) ×2500 and (C) Nano-HS ×25,000 and (D) ×25,000 before adsorption and after the adsorption (E) ×5000, (F) ×2500, nano-HS (G) ×200,000 and (H) ×200,000.

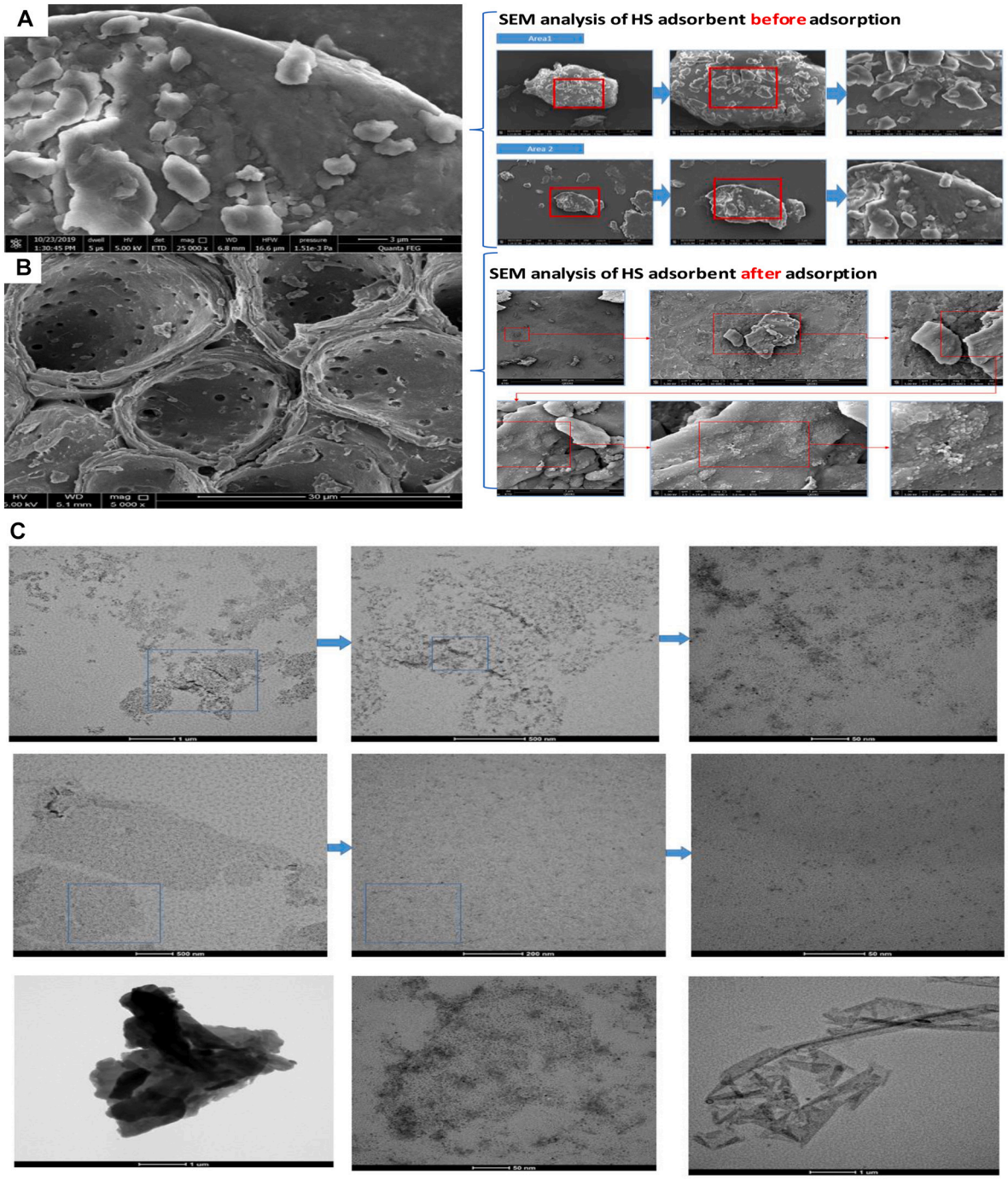

Fig. 5. SEM images of (A) HS adsorbent before adsorption, (B) HS adsorbent after the CV adsorption (C) TEM analysis of nano-HS, and (D) EDX analysis of nano-HS.

A specific area was further examined in depth to have a further visualization of the adsorbent structure as shown in Fig. 5A and 5B. Both adsorbents exhibited an irregularly shaped particle with a rough surface and deep cavities. Additionally, the particles possessed voids and bumps within their structure, which were accessible for the adsorption of CV. This is a favorable characteristic as it can increase the adsorption of CV onto the matter. Additionally, it is also possible to visualize various regions for CV ions accumulation, where mass adsorption of CV took place. From FTIR, various functional groups of HS were identified which facilitated the binding of CV dye onto the surface. Due to the complexity of the HS surface, it was assumed that CV could not move along the surface; hence, the surface diffusion into the adsorbent's particle was disregarded and considered negligible. It was assumed that the intra-particle diffusion took place due to the effective pore volume diffusion and when the CV was trapped within the pores.

3.3. TEM analysis

Further observations of the nano-HS structure were conducted by TEM analysis as shown in Fig. 5C. The size of the adsorbent and the inner pore distribution was not easily observed by SEM analysis; therefore, the TEM analysis was accomplished to further enhance the physical understanding of the adsorbent. Fig. 5C shows the TEM images as a well-developed porous structure of the adsorbent that is homogeneously

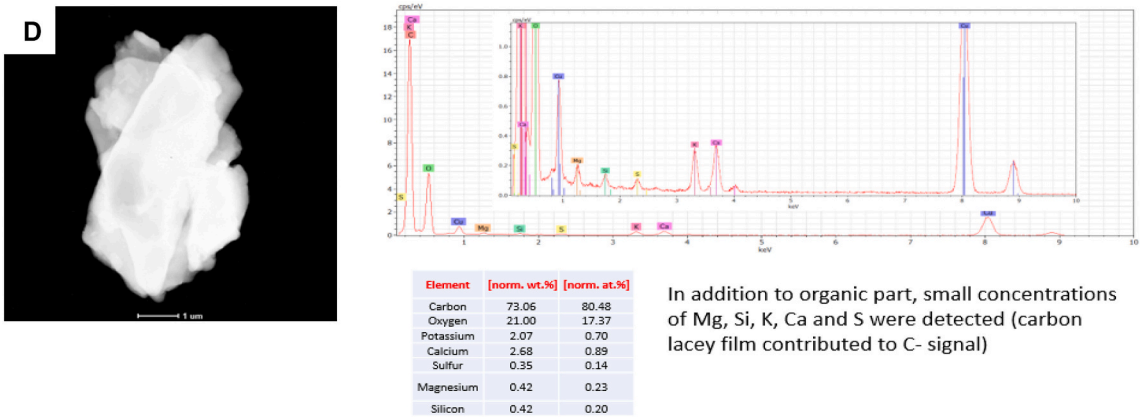

Fig. 5. (*continued*).

distributed. Additionally, the nano-HS exhibits an aggregated irregular surface with a high number of microspores and crevices at the surface. The nano-HS appeared as a conglomerate of very fine yet elongated particles as seen in Fig. 5C. Additionally, the TEM also suggests that the nanoparticles are present in cluster form of HS. Additionally, the TEM images confirmed the heterogeneity of nano-HS adsorbent and irregular region of the adsorption process of the CV, which can see as the darker region in Fig. 5C. In general, the TEM images in high magnification show that the particles have the tendency to agglomerate. Additionally, some areas also appeared as long irregular rod-like structures. Le et al. [64] found similar results, in which the spherical structure of Fe_3O_4/ZnO nanoparticles helped in the degradation of CV. While Gopi et al. [65] noticed rod-like structure in chitin nanoparticles whiskers facilitated CV adsorption.

3.4. Effect of the pH on the adsorption capacity

It is clearly shown from Fig. 6A that the CV removal percentage increases with increasing pH from 2 to 8 and does not significantly increase at a pH value higher than 8. However, pH 10 was reported to be the optimum pH. The pH_{ZPC} (the total positive charges that are equal to the total negative charges) exhibited a negative zeta potential value at all studied pH values. It was shown that there was no isoelectric point. The pH values and the zeta potentials were as follows: at pH = 3, −11 mV; pH = 4, −12 mV; pH = 6, −35 mV; pH = 8, −34 mV; pH = 10, −41 mV. The adsorption of CV onto HS is influenced by the pH solution. The pH of the solution governs the interaction between CV and the adsorbent, thus a change in pH solution directly influences their interaction and the ionizability of the functional groups. This could be explained due to the electrostatic interaction between positively charged CV and the negatively charged on the adsorbent's surface [23]. Additionally, at low pH, the biosorption of CV is noted to be low due to the concentration of H^+ ions present, which results in repulsion between the CV ions eventually resulting in low adsorption [27]. As the pH increased, more negatively charged functional groups were accessible resulting in an increase in adsorption and a decrease in repulsion between the cations and adsorbents. Similar findings were also observed by Doğan et al. [40], who elucidated that negatively charged adsorbent, was favorable for CV adsorption. While on the other hand, Dabagh et al. [66] reported no significant difference in adsorption capacity of CV onto novel Fe_3O_4-graphene biochar composite and *Carpobrotus edulis*. Moreover, as the pH increased, the CV adsorption onto the adsorbents reached up to 91% as seen in Fig. 6A. It was also deduced that the pH of the solution provides a driving force to surpass the mass transfer's resistance between the CV ions and the adsorbent. Additionally, empty sites at pH 8 and 9 were almost occupied as a result the reaction reached its equilibrium.

3.5. Adsorption mechanisms

Fig. 6B proposes a schematic illustration of how CV ions might have bonded on the HS surface. Due to the complex chemical structure and the presence of many binding sites of the HS shell, it is expected that CV can easily be adsorbed onto the surface. It can be assumed that ion exchange, electrostatic bond, and hydrogen bonding can be the principal mechanism of CV removal. The major components of such polymeric material shells are lignin, cellulose, and other phenolic compounds. From the nature of the material, as discussed earlier, it can be speculated that lignin and cellulose are the active ion-exchange compounds and phenolic groups present in the shell are the active site of adsorption activity [67]. Since the CV ions are positively charged, the uptake of the CV molecule onto the external surface of the HS or HS-nano would decrease the negativity charges on the adsorbent. Fig. 6C illustrates the possible mechanism of CV adsorption onto HS and nano-HS. According to the FTIR results, the charged molecules of CV were adsorbed by the various functional groups onto the HS or nano-HS, mainly C═O, C═C, C—O, and the —OH that were available from the adsorbents. Various adsorption mechanisms would be involved, namely hydrogen bonding, electrostatic attraction, π-π interaction, and n-π interaction [68]. As a result, the hydrophobicity of the adsorbents will be increased. Furthermore, as revealed in Fig. 6C, the CV adsorption onto HS starts with fast transportation of CV to the liquid film from the bulk solution, which can be attributed to the intense mixing throughout the experiment. After that, the negatively charged outer surface will readily attract the positively charged CV leading to a moderate/fast channel diffusion.

$$HS–OH \rightleftharpoons HS–O^- + H^+$$

$$HS–O^- + CV^+Cl^- \rightleftharpoons HS–O–CV^+$$

$$HS–OH + CV^+Cl^- \rightleftharpoons HS–O–CV + HCl$$

The CV equilibrium configurations, reactivity, and interactions onto nano-HS were proposed based on the conceptual density functional theory and the discussion of El Haouti et al. [70]. El Haouti et al. [70] investigated the adsorption mechanisms of two cationic dyes, Toluidine Blue (TB) and CV onto a nano-clay. Fig. 7 shows various parameters that were used to describe the chemical reactions. Eq. (1)–(3) represents the one-electron energies for the mentioned parameter of the highest occupied molecular orbital (HOMO) and lowest unoccupied molecular orbital (LUMO). The change in the chemical stasis of CV molecules on the nano-HS surface is illustrated in Fig. 7 from various orientations. The adsorbed molecules of CV cations had a comparatively lower adsorption rate (33%) formed a single layer. During the adsorption process, the aromatic rings of CV molecules are positioned towards the nano-HS surface. The interconnection between the H-atom of the —CH_3 groups

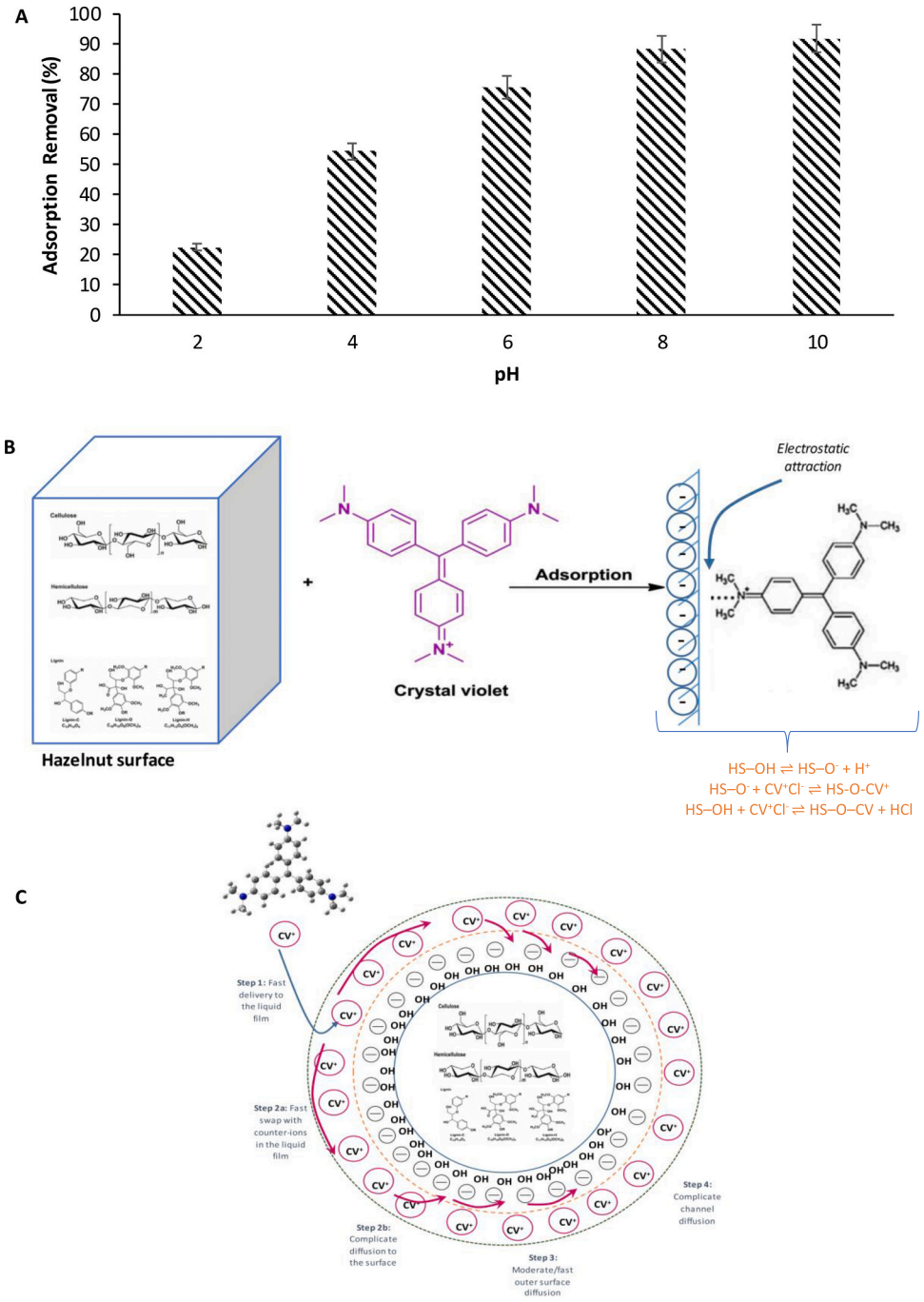

Fig. 6. A. The effect of pH on adsorption removal onto HS at different pH B. A schematic illustration of the interaction between CV ions and HS surface C. Proposed CV adsorption onto HS
Modified from Krasilin et al. [69].

of CV molecule and the nano-HS surface will be maximized due to the orientation of the aromatic moieties. The monolayer formation specifies that the adsorption was a chemisorption process that also agrees with the findings from the adsorption experiments.

Fig. 8A-C shows the adsorption mechanism of the CV into the intra/intermolecular hydrogen bonding pattern of cellulose structure [71], hemicellulose, and lignin [68], and the proposed configurations of CV adsorption onto nano-HS. This could be through face-to-face adsorption, single edge adsorption – cellulose, single edge adsorption – hemicellulose, single edge adsorption – lignin, face-to-face adsorption-loaded CV, and single edge adsorption – cellulose, hemicellulose, and lignin [70].

As the load increases to 66% and 100%, some adsorbed molecules would either form a flat orientation by settling flat on the basal surface while some may form a combination of tilted and random piles. The neat positive charge that is present on the studied CV ions, is not limited to the N atom but delocalized on the whole CV. Usually, the electrostatic and secondarily van der Waals interactions between CV and the oxygen atoms of the cellulose, hemicellulose, and lignin are predominantly attractive. This also indicates high dispersion of the CV and chemically electrical interactions between CV and nano-HS surface (π- π stacking, hydrogen bond, etc.). Additionally, the free conjugated electrons in CV play an essential part in the adsorption process by the interfacial interactions between CV molecules and cellulose, hemicellulose, and lignin components in the nano-HS surface. The energy components that

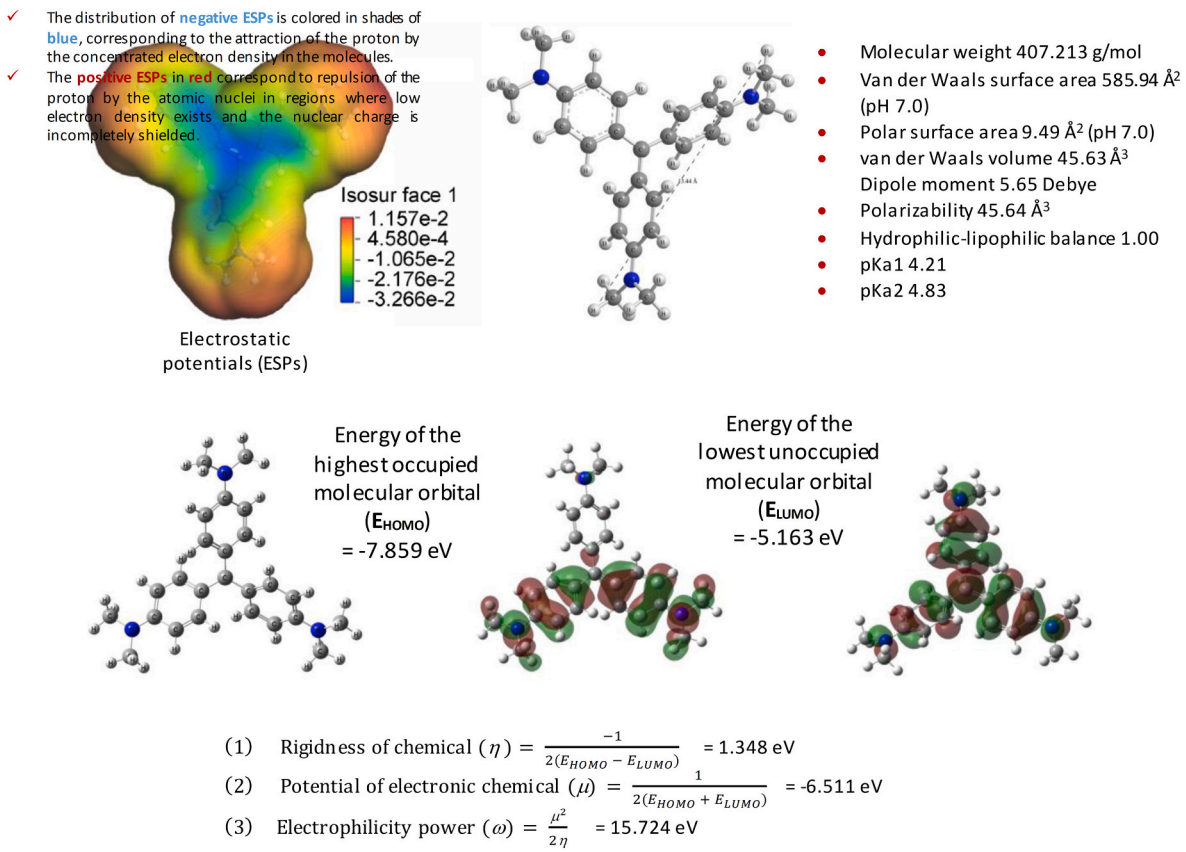

(1) Rigidness of chemical $(\eta) = \frac{-1}{2(E_{HOMO} - E_{LUMO})}$ = 1.348 eV

(2) Potential of electronic chemical $(\mu) = \frac{1}{2(E_{HOMO} + E_{LUMO})}$ = -6.511 eV

(3) Electrophilicity power $(\omega) = \frac{\mu^2}{2\eta}$ = 15.724 eV

Fig. 7. E_{HOMO} and E_{LUMO} and the Electrostatic potentials (ESPs) of CV [70–73].

were considered during the adsorption were both bonded and non-bonded interactions such as electrostatic and van der Waals involved in interaction energy.

3.6. *Effect of concentration on the adsorption capacity of HS and nano-HS*

The amount of the CV ions adsorbed on the adsorbent is a function of concentration at equilibrium. Therefore, increasing the initial CV concentration caused the CV adsorption onto HS and nano-HS to increase. This is also predictable as it suggests the mass transfer of CV on the available adsorption sites on HS surfaces. As the concentration increased the adsorption capacity of HS also increased as seen in Fig. 9. The adsorption capacity on HS increased from from19.77 mg/g to 325.09 mg/g and 20 mg/g to 304 mg/g on nano-HS. Additionally, there was a notable increase in the adsorption capacity from 20 mg/L to 500 mg/L. This could be due to the high driving and attractive forces such as electrostatic force and van der Waals force between the CV and the adsorbent molecules and on the adsorbents, sites surface [61]. Additionally, the fast diffusion of CV onto HS can also be associated with the rapid pore diffusion into the intraparticle matrixes, which consists of various chromophore groups as identified earlier that caused equilibrium rapidly [52]. Furthermore, the rapid increase in CV adsorption on HS is also due to a high driving force for CV ions transfer, which was maximized in a concentrated solution [74]. It was found that the adsorption capacity was better with a more concentrated solution [40]. However, the adsorption capacity declined from 700 mg/L, which can be due to no vacant sites available on HS surface, this indicates that the sites on the adsorbent have reached saturation and therefore, cannot adsorb more CV. In other words, the decrease in adsorption rate was caused due to an increase in the surface loading of CV ions, thus initially the adsorption was very rapid and high then a slower adsorption rate was followed due to the gradual decrease in the adsorption site. The highest adsorption capacity is 325.09 mg/g and 304 mg/g in Fig. 9 and 4.8 at 500 mg/L of the initial dye of CV. The intraparticle diffusion process may give information regarding the adsorption mechanism of CV onto the adsorbents. Moreover, Fig. 9 illustrates a tetra-linear graph that implies that in the adsorption mechanism there were four major steps, namely (i) the CV molecules were attracted as a monolayer or multilayer at the external surface of the adsorbent. For the HS, the pore size was bigger than the nano-HS, indicating the possibility of the CV molecules getting inside the pores, which were slightly below the surface, (iii) inner pores adsorption by the CV molecules, and (iv) equilibrium and the possibility of desorption at high concentration [75]. Table 2 shows a compilation of various studies that used agricultural waste to remove dyes and their maximum adsorption capacity. Franco et al. [52] found a similar mechanism of CV adsorption onto pecan pericarp as well as Karaçetin et al. [42] also found a similar trend of methylene blue adsorption onto HS.

Two-way ANOVA was performed to authenticate the data for the effect of concentration and pH on the adsorption process. According to Table 3, the *P*-value for the effect of pH for both HS and nano-HS was less than 0.05, indicating the reactions were significantly different. For the effect of initial concentration, the pH value for nano-HS was less than 0.05, while F-value was greater than F critic. This showed that the adsorption of CV onto nano-HS was significantly affected by the effect of the initial concentration of CV while for HS the P-value was greater than 0.05, implying that the effect of initial dye concentration was not significantly affected.

In Fig. 9, at a low concentration region (initial CV concentration < 200 mg/L) the CV molecules form a monolayer coverage on the adsorbents surface until all the available sites are saturated. On the other hand, by increasing the CV concentration higher than 400 mg/L, an inflection point in the isotherm can be observed. This increase in CV

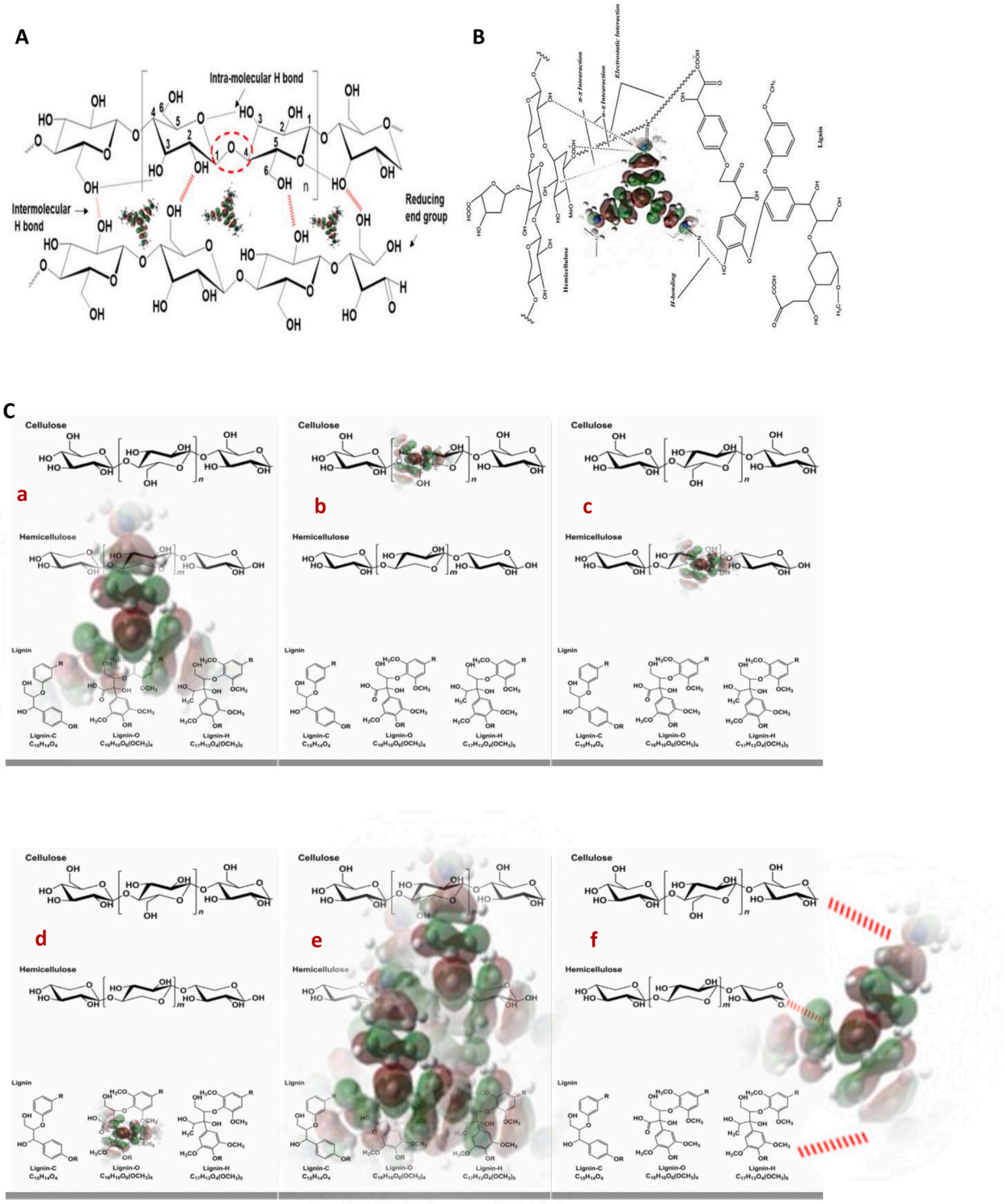

Fig. 8. A. Adsorption mechanism of the CV into the intra/intermolecular hydrogen bonding pattern of cellulose structure [71], B. The CV molecules interaction with hemicellulose, and lignin [68], and C. Proposed configurations of CV adsorption onto nano-HS. (a) face-to-face adsorption, (b) single edge adsorption – cellulose, (c) single edge adsorption – hemicellulose, (d) single edge adsorption – lignin, (e) face-to-face adsorption-loaded CV, (f) and single edge adsorption – cellulose, hemicellulose, and lignin
Modified from Ref. [70]).

uptake may specify that the adsorption mechanism has changed to a multilayer adsorption step. Fig. 10, illustrates the monolayer-multilayer adsorption of CV onto the adsorbent. Two active sites must be reflected, namely the original active sites at the adsorbent surface and novel active sites (i.e. in succession adsorbed onto previously adsorbed CV molecules) [76], as follows:

$$CV + \equiv S \leftrightarrow^{K1} CV \equiv SK1 = \frac{[CV \equiv S]}{[CV][\equiv S]} \text{First adsorption layer} \quad (4)$$

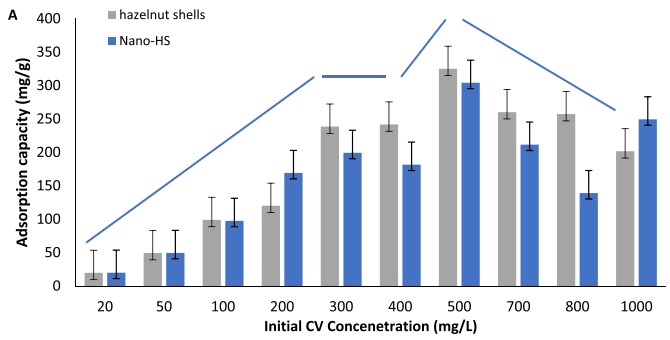

Fig. 9. The effect of initial dye concentration on the adsorption capacity of CV onto HS and nano-HS.

Table 2
Adsorption capacity of different sorbents for cationic dyes removal.

Reference	Adsorbent	Adsorption capacity (mg/g)
[18]	Mango stone	352.790
[19]	Tea residue	39.34
[20]	*Cucumis sativus*	33.32
[22]	Potato (*Solanum tuberosum*) plant wastes	52.60
[22]	Potato (*S. tuberosum*) plant wastes	33.3
[23]	Date palm leaves	37.736
[24]	Agro-industrial wastes	66.0
[25]	Peanut hull waste biomass	100.6
[26]	Prepared activated carbon from sugarcane bagasse soot	280
[27]	Water hyacinth	322.580
[28]	Lemongrass residue	36.10
[65]	Chitin nanowhiskers from shrimp shell	39.560
Current study	HS	325.90
Current study	Nano-HS	304.15

Table 3
Analysis of variance for effect of pH and initial concentration on CV adsorption onto HS and nano-HS.

	P-value	F-value	F-critical
pH (HS and nano-HS)	0.0011	24.87	5.32
Effect of initial concentration (Nano-HS)	0.04	4.92	4.41
Effect of initial concentration (HS)	0.06	4.09	4.41

$$CV + CV \equiv S \leftrightarrow^{K2} CV_2 \equiv S\ K2 = \frac{[CV_2 \equiv S]}{[CV][CV \equiv S\,]} \text{Second adsorption layer} \quad (5)$$

$$CV + CV_2 \equiv S \leftrightarrow^{K3} CV_3 \equiv S\ K3 = \frac{[CV_3 \equiv S]}{[CV][CV_2 \equiv S\,]} \text{ Third adsorption layer} \quad (6)$$

$$CV + CV_{n-1} \equiv S \leftrightarrow^{Kn} CV_n \equiv S\ Kn = \frac{[CV_n \equiv S]}{[CV][CV_{n-1} \equiv S\,]} \text{nth adsorption layer} \quad (7)$$

where, CV is a crystal violet molecule, ≡S is a free surface adsorbent site, CV_n≡S is a multilayer complex at the surface, and K1, K2, K3, …, Kn are the equilibrium constants related to each "i" layer, respectively.

Besides, a strong dependence from the adsorption capacity with the temperature can be observed in Fig. 11 especially at high CV concentrations. This is clearly shown for the HS adsorbent comparing to the nano-HS. However, by increasing the solution temperature the adsorption curves illustrate a significant increase in this inclination. This shows that multilayer adsorption is significantly favored by the temperature. In conclusion, the CV adsorption process onto HS could happen by two different adsorption mechanisms, depending on the experimental conditions such as the solution temperature and the initial CV concentration.

3.7. Effect of temperature

Fig. 11 shows the influence of temperature on the adsorption capacity of HS and nano-HS. The adsorption of CV on HS favored endothermic conditions. In general, the increase in temperature also increased adsorption capacity. For example, at 25 °C 282.11 mg/g of CV was adsorbed as compared to 335.50 mg/g at 45 °C. An increase in adsorption capacity can be due to the increase in the diffusion rate of the adsorbate molecules throughout the external and internal boundary of the internal pores of HS due to the decrease in solution viscosity. Additionally, an increase in temperature also influences the biosorption activity by increasing the kinetic energy of the solute as well as the surface activity. Additionally, it is also possible that high temperature favored the interaction between chromophore groups such as hydroxyl and carboxylic of the hazelnut shell and the cationic group on CV dye. Furthermore, electrostatic attraction forces and hydrogen bonding between the —OH group of HS shell and nitrogen atom in CV might have taken place at high temperatures [40]. Similar findings were observed in a study by Derafa, Zaghouane-Boudiaf [74], who investigated the adsorption capacity of CV and concluded that the adsorption capacity was enhanced at a higher temperature as well as Karaçetin et al. [42] who concluded that an increase in temperature was favorable for MB adsorption onto HS. While on the other hand, nano-HS favored exothermic conditions, as observed from Fig. 11 at 25 °C, 567.45 mg/g was the highest adsorption rate achieved which decreased to 291.36 mg/g and 109.29 mg/g at 35 °C and 45 °C respectively. This can be explained due to a physical modification of the adsorbent that might have taken place at high temperatures, the pores might have surged, which caused a decrease in adsorption capacity.

3.8. Adsorption isotherm

The adsorption studies aid in outlining how adsorbate molecules interact with an adsorbent. Four isotherm models, Langmuir, Freundlich, Dubinin-Radushkevich, and Temkin isotherm were studied in this study. These isotherm models will show the dispersal of dyes ions between the solid and liquid phase which helps in providing qualitative information for any adsorption process. Table 4 shows the four isothermal model and their relevant calculated parameters, constants, and correlation coefficients. Langmuir isotherm presumes that the adsorption of CV on the HS and nano-HS occurred on a homogenous surface and no further adsorption could occur. The correlation coefficient (R^2) was close to 1 for HS (0.92–0.93), for the Langmuir isotherm, and for nano HS it was between 0.90 and 0.96, suggesting that the Langmuir isotherm could be used to explain the adsorption of CV onto HS. Furthermore, for HS the maximum adsorption capacity (Q°) indicated that the maximum adsorption capacity increased as the temperature from 133.33 mg/g at 25 °C while 181.82 mg/g at 45 °C. However, for the nano-HS, the maximum adsorption capacity decreased as the temperature increased from 294.12 at 25 °C, to 133.33 mg/g at 45 °C. Additionally, the affinity between the adsorbate and adsorbent is denoted by K_L, which demonstrated a strong binding at 25 °C for HS while for nano-HS it showed high affinity at 45 °C. Freundlich isotherm assumes that the adsorption took place on a heterogeneous and multilayer surface [77]. The adsorption capacity (K_F) of HS and nano-HS showed an overall increase as the temperature increased from 4.10 $(mg/g)/(g/L)^{1/n}$ at 25 °C and 3.33 $(mg/g)/(g/L)^{1/n}$ for nano-HS, which increased to 4.40 $(mg/g)/(g/L)^{1/n}$ and 4.07 $(mg/g)/(g/L)^{1/n}$ at 45 °C.

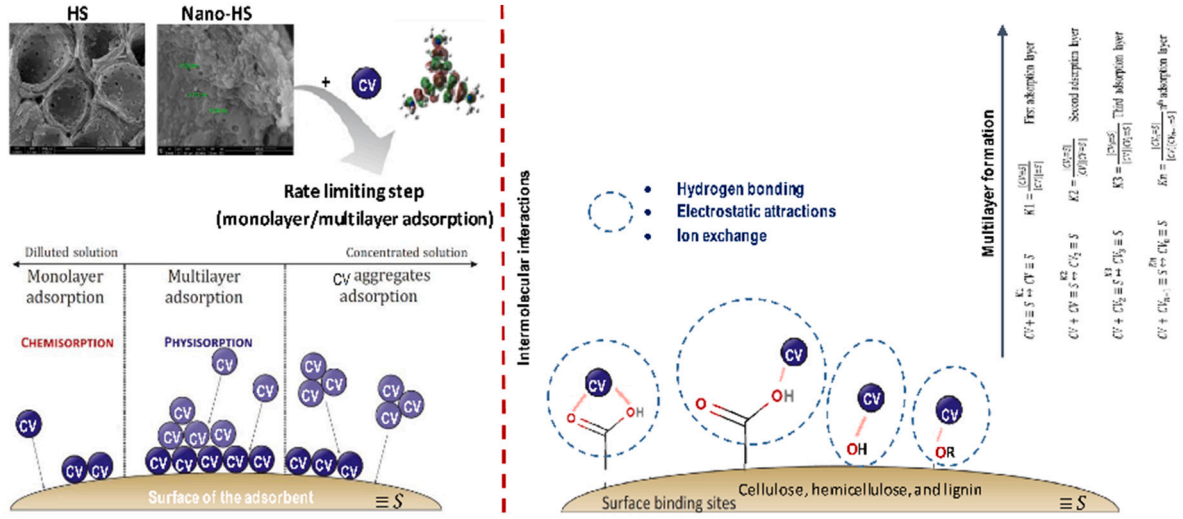

Fig. 10. Monolayer-multilayer adsorption of CV onto SH or nano-HS (modified from Scheufele et al. [76]).

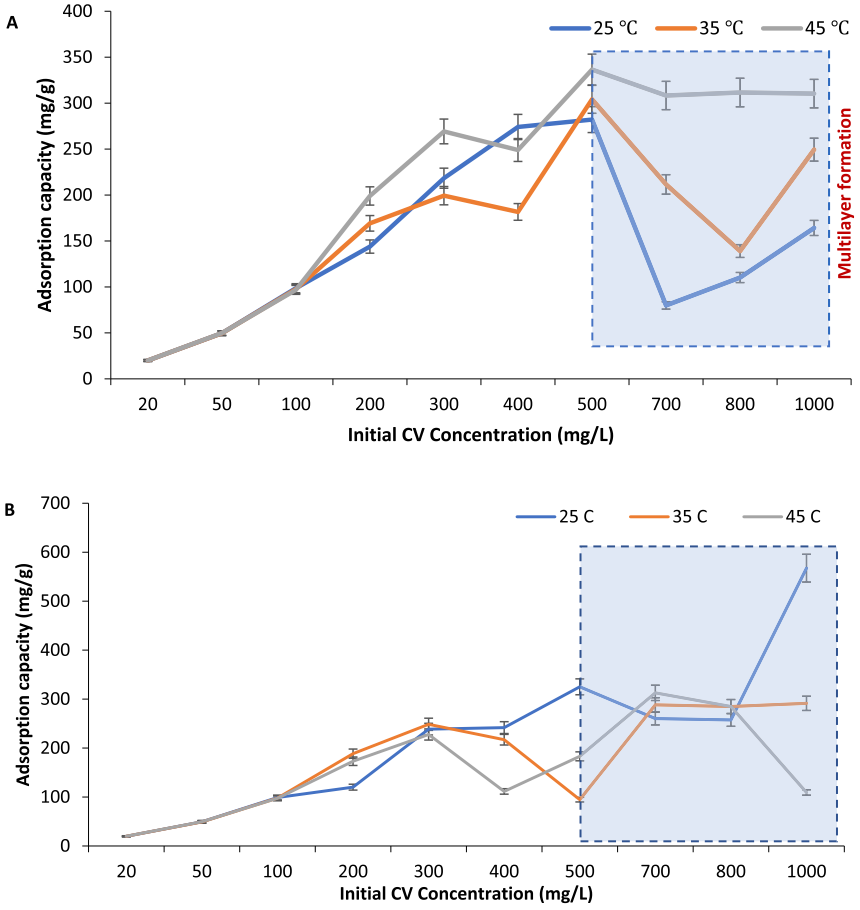

Fig. 11. The effect of temperature on adsorption capacity on A. HS and B. nano-HS.

The highest coefficient relation for HS was 0.85 while nano HS was reported to be 0.89 at 35 °C. The constant Freundlich n is referred to as the adsorption intensity of adsorbents. The *n* value indicates whether the reaction was chemical or physical adsorption. The values for both HS and nano HS were greater than 1; indicating the adsorption was best explained as physical adsorption. Generally, the value of $\frac{1}{n}$ was higher than 1, which indicated the adsorption process was favorable [22]. The Dubinin-Radushkevich (D-R) was not suitable to describe the adsorption process of CV onto HS and nano-HS as the R^2 value was between 0.65 and 0.73 for HS, and 0.62–0.80 for nano-HS. Additionally, D-R is considered more applicable for a single solute adsorption type due to its characterization of good performance and easy mathematical equations [49]. Lastly, Temkin isotherm was also not best fitted, as the R^2 values were 0.34–0.87 for HS and 0.50–0.95 for nano-HS. Ahmed et al. [57], also studied the removal of CV and rejected Temkin due to low correlation efficiency. Tran et al. [51] evaluated the methylene blue

Table 4
The parameters of adsorption isotherm of the CV adsorption onto the HS and nano-HS.

HS								
Temperature	Langmuir				Freundlich			
(°C)	Q^{o}_{max} (mg/g)	K_L (L/mg)	R^2		K_F ((mg/g)/(g/L)$^{1/n}$)	n	1/n	R^2
25	133.33	3.12	0.93		4.10	5.57	1	0.56
35	151.52	2.75	0.93		4.06	4.40	3	0.85
45	181.82	5.50	0.92		4.40	4.11	3	0.84
Temperature (°C)	Dubinin-Radushkevich				Temkin			
	Q_D (mg/g)	B_D (mol^2/kJ^2)	E (kJ/mol)	R^2	B (J/mol)	bt	A_T (L/mg)	R^2
25	12.23	-5×10^{-8}	144.05	0.65	15.48	160.03	0.77	0.34
35	18.11	-4×10^{-8}	168.39	0.73	21.91	116.82	0.59	0.71
45	15.59	3×10^{-8}	223.72	0.73	30.38	87.02	0.63	0.87
Nano-HS								
Temperature	Langmuir				Freundlich			
(°C)	Q^{o}_{max} (mg/g)	K_L (L/mg)	R^2		K_F ((mg/g)/(g/L)$^{1/n}$)	n	1/n	R^2
25	294.12	0.33	0.96		3.99	3.33	0.30	0.82
35	188.68	0.098	0.94		4.04	3.49	6	0.89
45	133.33	5.35	0.90		4.07	4.76	3	0.78
Temperature (°C)	Dubinin-Radushkevich				Temkin			
	Q_D (mg/g)	B_D (mol^2/KJ^2)	E (kJ/mol)	R^2	B (J/mol)	bt	A_T (L/mg)	R^2
25	31.49	-2×10^{-7}	241.79	0.80	41.02	60.39	0.26	0.60
35	9.94	-9×10^{-8}	200.77	0.70	33.43	76.58	0.39	0.95
45	7.80	-3×10^{-8}	154.50	0.62	20.11	131.42	0.63	0.50

adsorption on carbonaceous hydrochar and found that the adsorption process was best described by the Langmuir model. From the data tabulated in Table 4, it is evident that the adsorption process of HS and nano-HS can be best described using the Langmuir model. This model assumes that the adsorption was on a monolayer without any internal interaction between adsorbed ions. Additionally, the adsorption occurred on a homogenous site. Additionally, the maximum adsorption capacity for HS was 181.82 mg/g and 294.12 mg/g for nano-HS. Additionally, it is also evident nano-HS is a better adsorbent for CV. This can be due to the formation of deeper cavities and the general morphology of nano-CV. Table 5 shows a comparison of the current study against other studies that have used different adsorbents to remove CV from an aqueous solution. The table shows that HS had commendable adsorption capacity in contrast to other agricultural waste. Thus, it can be concluded HS (181.82 mg/g) and nano-HS (294.12 mg/g) can prove to be excellent adsorbents to remove CV. By comparing with other low-cost adsorbents, it is evident that the value of Q_{max} obtained in the current study is higher in contrast to other reported adsorbents. Moreover, HS can be considered as an applicable adsorbent for the removal of other cationic dyes, which can be attributed to the fact that cationic dyes adsorption decreases in an acidic environment (i.e. low pH value) due to the excess existence of H^+ ions that will compete with the cationic dyes for the available active sites on the adsorbent surface. Increasing the solution pH will increase the removal efficiency due to the less electrostatic repulsion between the adsorbent surface and the positively charged cationic dyes. In addition, due to the presence of OH^- and COO^- functional groups, the adsorption of cationic dyes is more favored at pH > pH_{pzc}. Furthermore, the carboxyl groups present on the surface of HS as a major negative functional group will bear with the cationic dyes and enhance its adsorption. Cellulose-based adsorbents like HS can adsorb cationic dyes through columbic attraction because of the negatively charged surface that is acquired by HS-cellulosic material in contact with water. Our results are in line with Ferrero [41], who investigated the removal of methylene blue from an aqueous medium by HS and found that the Langmuir isotherm model best fitted the experimental data, and the adsorption capacity increases with increasing the pH value. Similarly, Doğan et al. [40] found that removal of cationic dyes by HS increased significantly with increasing the initial concentration and temperature. This can be attributed to the fact that changing the solution temperature for the adsorption of cationic dye leads to the increase in the diffusion rate of dye molecules across the external boundary layer as well as in the HS internal pores. The applicability of HS on the adsorption of different cationic dyes was supported by Karaçetin et al. [42], who observed that cationic dye adsorption is an endothermic and spontaneous process.

Table 5
Various studies on CV adsorption using agricultural waste.

Adsorbents	Adsorbate	Q°_{max} (mg/g)	Isotherm model	References
Fly ash	CV	172.41	Langmuir	Liu et al. [12]
Mango stone	CV	352.79	Langmuir	Shoukat et al. [18]
Orange peel	CV	138.9	Langmuir	Ahmed et al. [57]
Chitin nanowhiskers from shrimp shell (ChNW)	CV	39.56	–	Gopi et al. [65]
Urtica dioica leaf powder	CV	1790	Langmuir	Derafa, Zaghouane-Boudiaf [74]
Green Alginate/Pectin nanocomposite	CV	619.22	Langmuir	Mirza & Ahmed [78]
Nano-hazelnut shells (nano-HS)	CV	294.12	Langmuir	This study
Hazelnut shells (HS)	CV	181.82	Langmuir	This study

3.9. Thermodynamic studies

Thermodynamic parameters for instance change in entropy (ΔS°), changes in enthalpy (ΔH°), and the Gibbs free energy (ΔG°) can be used to indicate the thermodynamic viability of the adsorption process. The positive (ΔH°) (Table 6) for HS, indicates that the reaction was endothermic. As the temperature increased the value of ΔG° also increased, indicating that the reaction was favorable and spontaneous, and the favorability declined as the temperature increased. While the positive

Table 6
Thermodynamic parameter of CV adsorption onto HS and nano-HS.

Temperatures	ΔG° (kJ/mol)	ΔH° (kJ/mol)	ΔS° (J/mol·K)
nano-HS			
25 °C	3.223	−47.541	−170.35
35 °C	4.927		
45 °C	6.630		
HS			
25 °C	−2.488	21.912	81.88
35 °C	−3.307		
45 °C	−4.126		

value of ΔS° indicated a good affinity between CV and HS. This can be due to several various forces such as van der Waals, electrostatic [79,80]. The negative value of ΔH° signifies that the CV adsorption onto nano-HS was an exothermic reaction. The high value of ΔS° further indicated a good affinity of CV ions on to HS nanoparticles which caused an increase in randomness [50]. Lastly, the positive value of ΔG° (greater than −20 kJ/mol) indicates that the reaction requires, energy input, and physical absorption was reconfirmed regardless of the temperature. Similar findings were found in a study by Silva et al. [30].

The Gibbs free energy of nanoparticles increases as temperature increases. Furthermore, the positive values of the adsorption Gibbs free energy are higher at higher temperatures, which suggests adsorptions become less favorable at higher temperatures. In addition, there is an inverse relationship between adsorption Gibbs free energy and diameter (d) of the particle size at a given temperature [81]. The result indicates that the nano-HS has a negative effect on the entropy and the enthalpy.

This could be explained as nano-HS can produce a strong surface effect, and the effect of the surface area on the adsorption Gibbs free energy is substantial. This means that the chemical potential at the nanoscale level (μ) should reflect both the bulk (μ^B) and the interfacial (μ^I) parts, as

$$\mu = \mu^B + \mu^I = \mu^B + \frac{4\sigma V}{d} \tag{8}$$

where V is the molar volume of the nano-adsorbent, and σ is the surface tension.

Therefore, the Gibbs free energy of nanoparticles could be as,

$$\Delta G^\circ = (\Delta G^\circ)^B + (\sigma^\infty - \sigma)\frac{4V}{d} \tag{9}$$

where, σ^∞ is the surface tension of the adsorption product in a saturated state, denotes adsorption equilibrium.

In the current study, there could be an increase in the surface tension after adsorption, which means that σ^∞ is bigger than σ, and the Gibbs free energy of nanoparticles becomes more positive in the case of nano-HS (Fig. 12).

3.10. Desorption studies/regeneration of HS and nano-HS

The desorption studies were performed to assess the reusability of HS and nano-HS to remediate CV from an aqueous solution. The HS and nano-HS after the adsorption experiments were subjected to CV desorption using ethanol solution and acetic acid (1.0 M for 24 h). The repeatability study was conducted three times. 88.01% and 70.86% were the average desorption removal efficiency recorded, respectively, which indicated that both adsorbents could successfully be used repeatedly for CV-dye adsorption. This can be due to the strong interaction between CV and nano-HS in comparison to HS.

3.11. Cost analysis

When comparing the efficiency of an adsorbent, the cost of the adsorbent plays a crucial role [83]. It is considered vital when determining the success of any adsorption treatment techniques. Usually, a sorbent is considered cost-effective when the material is available in nature or requires little to no modification to enhance its adsorption capabilities. In this study, a cost-effective method was used to remediate CV from an aqueous solution using an agro-waste. It aimed to use sustainable material by recycling hazelnut shells, which are typically

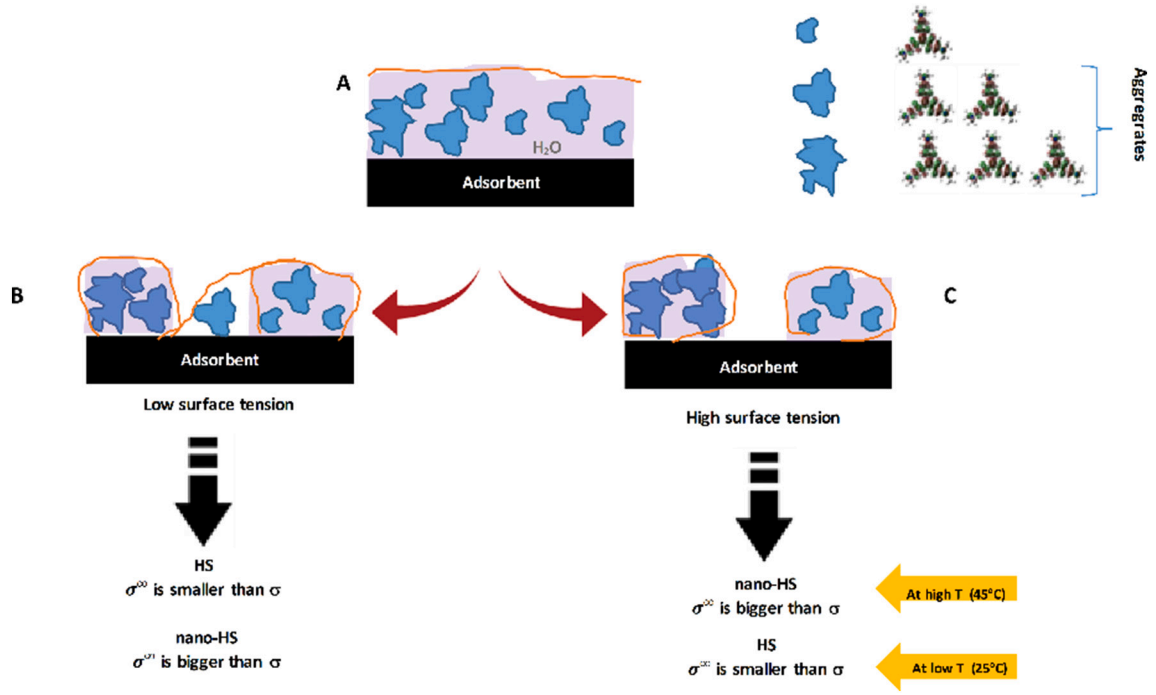

Fig. 12. Schematic illustrations of the nanoadsorption process and the effect of surface tension A. CV ions in the aqueous phase (single or aggregates), B. Low surface tension, CV ions bonded to the adsorbent, high wettability, and has an effect on the positioning of the CV, and C. High surface tension, low wettability, CV ions are swept by the liquid (modified from [82]).

discarded and regarded as waste. In addition, the chemicals such as HCl and NaOH that were used in the study were of very low concentration and volume. Electricity used while performing the experiment was the only cost that this study required. Additionally, by calculating the maximum adsorption capacity and comparing it with other viable options, it proved HS could be replaced as an effective adsorbent material to remove CV from an aqueous solution.

4. Conclusion

This study suggested HS as a successful adsorbent for CV removal. The adsorption process preferred a basic environment, which enhanced the surface structure of HS to enhance adsorption. Additionally, the various functional group identified from FTIR also played a major role. Before and after SEM, images revealed that HS was a heterogeneous, highly porous, and deep cavities surface, which helped in capturing CV ions onto the adsorbent. The presence of CV ions after adsorption confirmed the success of the adsorption binding of CV on the HS and nano HS adsorbent. Langmuir isotherm best describes the adsorption process for both HS and nano-HS with R^2 values higher than 0.90. The maximum adsorption capacity for HS was 181.82 mg/g and nano-HS was 294.12 mg/g. Moreover, the process followed an endothermic reaction for HS and exothermic for nano-HS. Based on these results, the adsorption process shows the successful ability of both adsorbents for removing CV from aqueous solution without consuming much cost, energy. This study offers a sustainable option by utilizing agricultural wastes that do not necessarily require modification to adsorb cationic dyes, and proving to be a suitable alternative for CV removal in wastewater treatment processes.

Declaration of competing interest

The authors declare that they have no known competing financial interests or personal relationships that could have appeared to influence the work reported in this paper.

Acknowledgement

The authors would like to thank the lab technician Mr. Abdul-Ali Moghaddasi for his effort and help. We greatly appreciate the assistance from the Central Laboratory Unit, Qatar University for their help in performing the SEM. Special thanks to Mrs. Mariam Khan and Mrs. Dana Da'na for their assistance in editing the drafts of the manuscript. Open Access funding provided by the Qatar National Library

References

[1] Y. Liu, Y. Zhao, W. Cheng, T. Zhang, Targeted reclaiming cationic dyes from dyeing wastewater with a dithiocarbamate-functionalized material through selective adsorption and efficient desorption, J. Colloid Interface Sci. 579 (2020) 766–777.
[2] H. Ben Mansour, O. Boughzala, D. Drid, D. Barillier, L. Chekir-Ghedira, R. Mosrati, Textiles dyes as a source of wastewater contamination: screening of the toxicity and treatment methods, J of Water Sci 24 (2011) 209–239.
[3] K. Belkassa, M. Khelifa, I. Batonneau-Gener, K. Marouf-Khelifa, A. Khelifa, Understanding of the mechanism of crystal violet adsorption on modified halloysite: hydrophobicity, performance, and interaction, J. Hazard. Mater. 415 (2021), 125656.
[4] C.R. Holkar, A.J. Jadhav, D.V. Pinjari, N.M. Mahamuni, A.B. Pandit, A critical review on textile wastewater treatments: possible approaches, J. Environ. Manag. 182 (2016) 351–366.
[5] D.A. Yaseen, M. Scholz, Textile dye wastewater characteristics and constituents of synthetic effluents: a critical review, Int. J. Environ. Sci. Technol. (2018), https://doi.org/10.1007/s13762-018-2130-z.
[6] L.D. Ardila-Leal, R.A. Poutou-Piñales, A.M. Pedroza-Rodríguez, B.E. Quevedo-Hidalgo, A brief history of colour, the environmental impact of synthetic dyes and removal by using laccases, Molecules 26 (2021) 3813, https://doi.org/10.3390/molecules26133813, 2021.
[7] C. Srikantan, G. Suraishkumar, S. Srivastava, Effect of light on the kinetics and equilibrium of the textile dye (Reactive Red 120) adsorption by *Helianthus annuus* hairy roots, Bioresour. Technol. 257 (2018) 84–91.
[8] S. Mani, R.N. Bharagava, Exposure to crystal violet, its toxic, genotoxic and carcinogenic effects on environment and its degradation and detoxification for environmental safety, Rev. Environ. Contam. Toxicol. Vol. 237 (2016) 71–104.
[9] R.N. Bharagava, S. Mani, S.I. Mulla, G.D. Saratale, Degradation and decolourization potential of an ligninolytic enzyme producing *Aeromonas hydrophila* for crystal violet dye and its phytotoxicity evaluation, Ecotoxicol. Environ. Saf. 156 (2018) 166–175.
[10] R. Fabryanty, C. Valencia, F. Soetaredjo, J. Putro, S. Santoso, A. Kurniawan, Y. Ju, S. Ismadji, Removal of crystal violet dye by adsorption using bentonite – alginate composite, J Environ Chem Eng 5 (6) (2017) 5677–5687.
[11] K. Foo, B. Hameed, Insights into the modeling of adsorption isotherm systems, Chem. Eng. J. 156 (1) (2010) 2–10.
[12] S. Liu, Z. Wang, J. Li, C. Zhao, X. He, G. Yang, Fabrication of slag particle three-dimensional electrode system for methylene blue degradation: characterization, performance and mechanism study, Chemosphere 213 (2018) 377–383.
[13] J. Chen, Y. Pu, C. Wang, J. Han, Y. Zhong, K. Liu, Synthesis of a novel nanosilica-supported poly β-cyclodextrin sorbent and its properties for the removal of dyes from aqueous solution, Colloids Surf. A Physicochem. Eng. Asp. 538 (2018) 808–817.
[14] A. Spagnoli, D. Giannakoudakis, S. Bashkova, Adsorption of methylene blue on cashew nut shell based carbons activated with zinc chloride: the role of surface and structural parameters, J. Mol. Liq. 229 (2017) 465–471.
[15] J.H. Kumari, P. Krishnamoorthy, T. Arumugam, S. Radhakrishnan, D. Vasudevan, An efficient removal of crystal violet dye from waste water by adsorption onto TLAC/chitosan composite: a novel low cost adsorbent, Int. J. Biol. Macromol. 96 (2017) 324–333.
[16] A. Djelad, A. Mokhtar, A. Khelifa, A. Bengueddach, M. Sassi, Alginate-whey an effective and green adsorbent for crystal violet removal: kinetic, thermodynamic and mechanism studies, Int. J. Biol. Macromol. 139 (2019) 944–954.
[17] X. Pang, L. Sellaoui, D. Franco, G. Dotto, J. Georgin, A. Bajahzar, et al., Adsorption of crystal violet on biomasses from pecan nutshell, para chestnut husk, araucaria bark and palm cactus: experimental study and theoretical modeling via monolayer and double layer statistical physics models, Chem. Eng. J. 378 (2019) 122101.
[18] S. Shoukat, H. Bhatti, M. Iqbal, S. Noreen, Mango stone biocomposite preparation and application for crystal violet adsorption: a mechanistic study, Microporous Mesoporous Mater. 239 (2017) 180–189.
[19] L.H.T. Nguyen, H.T.T. Nguyen, B.Q.G. Le, D. Dang M-H, T.T.T. Nguyen, N.X. D. Mai, T.L.H. Doan, Microwave-assisted solvothermal synthesis of defective zirconium-organic framework as a recyclable nano-adsorbent with superior adsorption capacity for efficient removal of toxic organic dyes, Colloid and Interface Science Communications (2021) (in press).
[20] H. Raza, I. Yildiz, F. Yasmeen, K.S. Munawar, M. Ashfaq, M. Abbas, M. Ahmed, H. A. Younus, S. Zhang, N. Ahmad, Synthesis of a 2D copper(II)-carboxylate framework having ultrafast adsorption of organic dyes, J. Colloid Interface Sci. 602 (2021) 43–54.
[21] P. Moharrami, E. Motamedi, Application of cellulose nanocrystals prepared from agricultural wastes for synthesis of starch-based hydrogel nanocomposites: efficient and selective nanoadsorbent for removal of cationic dyes from water, Bioresour. Technol. 313 (2020) 123661.
[22] N. Gupta, A. Kushwaha, M. Chattopadhyaya, Application of potato (*Solanum tuberosum*) plant wastes for the removal of methylene blue and malachite green dye from aqueous solution, Arab. J. Chem. 9 (2016) S707–S716.
[23] A. Ghazali, M. Shirani, A. Semnani, V. Zare-Shahabadi, M. Nekoeinia, Optimization of crystal violet adsorption onto Date palm leaves as a potent biosorbent from aqueous solutions using response surface methodology and ant colony, J Environ Chem Eng 6 (4) (2018) 3942–3950.
[24] H. Parab, M. Sudersanan, N. Shenoy, T. Pathare, B. Vaze, Use of agro-industrial wastes for removal of basic dyes from aqueous solutions, Clean Soil Air Water 37 (12) (2009) 963–969.
[25] N. Tahir, H. Bhatti, M. Iqbal, S. Noreen, Biopolymers composites with peanut hull waste biomass and application for crystal violet adsorption, Int. J. Biol. Macromol. 94 (2017) 210–220.
[26] L. Giusto, F. Pissetti, T. Castro, F. Magalhães, Preparation of activated carbon from sugarcane bagasse soot and methylene blue adsorption, Water Air Soil Pollut. 228 (7) (2017).
[27] M. Kulkarni, T. Revanth, A. Acharya, P. Bhat, Removal of crystal violet dye from aqueous solution using water hyacinth: equilibrium, kinetics and thermodynamics study, Resource-Efficient Technol 3 (1) (2017) 71–77.
[28] K. Putri, A. Keereerak, W. Chinpa, Novel cellulose-based biosorbent from lemongrass leaf combined with cellulose acetate for adsorption of crystal violet, Int. J. Biol. Macromol. 156 (2020) 762–772.
[29] K. Wang, N. Peng, J. Sun, G. Lu, M. Chen, F. Deng, et al., Synthesis of silica-composited biochars from alkali-fused fly ash and agricultural wastes for enhanced adsorption of methylene blue, Sci. Total Environ. 729 (2020) 139055.
[30] J. Silva, M. Rosa, P. Beck, E. Peres, G. Dotto, F. Kessler, F. Grasel, Preparation of an alternative adsorbent from *Acacia mearnsii* wastes through acetosolv method and its application for dye removal, J. Clean. Prod. 180 (2018) 386–394, https://doi.org/10.1016/j.jclepro.2018.01.201.
[31] A. Jamshaid, A. Hamid, N. Muhammad, A. Naseer, M. Ghauri, J. Iqbal, et al., Cellulose-based materials for the removal of heavy metals from wastewater - an overview, Chem. Rev. 4 (4) (2017) 240–256.
[32] P. Manzanares, Integrated hydrolysis, fermentation and co-fermentation of lignocellulosic biomass, Bioalcohol Produc (2010) 205–223.
[33] B. Yuan, M. Lu, K. Eskridge, L. Isom, M. Hanna, Extraction, identification, and quantification of antioxidant phenolics from hazelnut (*Corylus avellana* L.) shells, Food Chem. 244 (2018) 7–15.

[34] M. Uyan, F. Alptekin, D. Cebi, M. Celiktas, Bioconversion of hazelnut shell using near critical water pretreatment for second generation biofuel production, Fuel 273 (2020) 117641.
[35] H. Şenol, Biogas potential of hazelnut shells and hazelnut wastes in Giresun City, Biotechnol Reports 24 (2019) 00361.
[36] E. Hoşgün, D. Berikten, M. Kıvanç, B. Bozan, Ethanol production from hazelnut shells through enzymatic saccharification and fermentation by low-temperature alkali pretreatment, Fuel 196 (2017) 280–287.
[37] E. Demirkaya, O. Dal, A. Yüksel, Liquefaction of waste hazelnut shell by using sub- and supercritical solvents as a reaction medium, J. Supercrit. Fluids 150 (2019) 11–20.
[38] G. Gozaydin, A. Yuksel, Valorization of hazelnut shell waste in hot compressed water, Fuel Process. Technol. 166 (2017) 96–106.
[39] N. Kaya, Z. Yildiz, S. Ceylan, Preparation and characterization of biochar from hazelnut shell and its application properties for methylene blue dye, J. Polytech. 21 (2018) 765–776, 4.
[40] M. Doğan, H. Abak, M. Alkan, Adsorption of methylene blue onto hazelnut shell: kinetics, mechanism and activation parameters, J. Hazard. Mater. 164 (1) (2009) 172–181.
[41] F. Ferrero, Dye removal by low cost adsorbents: hazelnut shells in comparison with wood sawdust, J. Hazard. Mater. 142 (1–2) (2007) 144–152.
[42] G. Karaçetin, S. Sivrikaya, M. Imamoğlu, Adsorption of methylene blue from aqueous solutions by activated carbon prepared from hazelnut husk using zinc chloride, J. Anal. Appl. Pyrolysis 110 (2014) 270–276.
[43] R. Carletto, C. Fabiana, F. Bosco, F. Ferrero, Adsorption of Congo red dye on hazelnut shells and degradation with phanerochaete chrysosporium, Bioresour 3 (4) (2008) 1146–1155.
[44] M.A. Al-Ghouti, S.S. Dib, Utilization of nano-olive stones in environmental remediation of methylene blue from water, J. Environ. Health Sci. Eng. 18 (2020) 63–77.
[45] T. Cloete, Nanotechnology in Water Treatment Applications, Caister Academic, Wymondham, 2010.
[46] F. Akbal, N. El Alem, M.L. Taha, Cationic dyes adsorption by Na-montmorillonite nano clay: experimental study combined with a theoretical investigation using DFT based descriptors and molecular dynamics simulations, J. Mol. Liq. 290 (15) (2019), 111139.
[47] S. Farooq, A. Saeed, M. Sharif, J. Hussain, F. Mabood, M. Iftekhar, Process optimization studies of crystal violet dye adsorption onto novel, mixed metal $Ni_{0.5}Co_{0.5}Fe_2O_4$ ferrospinel nanoparticles using factorial design, J Water Process Eng 16 (2017) 132–141.
[48] M. Banerjee, R. Basu, S. Das, Cr(VI) adsorption by a green adsorbent walnut shell: adsorption studies, regeneration studies, scale-up design and economic feasibility, Process Saf Environ 116 (2018) 693–702.
[49] M.A. Al-Ghouti, D.A. Da'ana, Guidelines for the use and interpretation of adsorption isotherm models: a review, J. Hazard. Mater. 393 (2020), 122383.
[50] E. Lima, A. Hosseini-Bandegharaei, I. Anastopoulos, Response to "Some remarks on a critical review of the estimation of the thermodynamic parameters on adsorption equilibria. Wrong use of equilibrium constant in the van't Hoff equation for calculation of thermodynamic parameters of adsorption - J. Mol. Liq. 273: 425–434", J. Mol. Liq. (2019) 298–300, 280.
[51] T. Tran, A. Le, T. Pham, D. Nguyen, S. Chang, W. Chung, D. Nguyen, Adsorption isotherms and kinetic modeling of methylene blue dye onto a carbonaceous hydrochar adsorbent derived from coffee husk waste, Sci. Total Environ. 725 (2020) 138325.
[52] D. Franco, J. Fagundes, J. Georgin, N. Salau, G. Dotto, A mass transfer study considering intraparticle diffusion and axial dispersion for fixed-bed adsorption of crystal violet on pecan pericarp (*Carya illinoensis*), Chem. Eng. J. 397 (2020) 125423.
[53] T. Saleh, Simultaneous adsorptive desulfurization of diesel fuel over bimetallic nanoparticles loaded on activated carbon, J. Clean. Prod. 172 (2018) 2123–2132.
[54] T. Taflick, L. Schwendler, S. Rosa, C. Bica, S. Nachtigall, Cellulose nanocrystals from acacia bark–influence of solvent extraction, Int. J. Biol. Macromol. 101 (2017) 553–561.
[55] N. Kataria, V. Garg, Optimization of Pb (II) and cd (II) adsorption onto ZnO nanoflowers using central composite design: isotherms and kinetics modeling, J. Mol. Liq. 271 (2018) 228–239.
[56] E. Pehlivan, T. Altun, S. Cetin, M. Iqbal Bhanger, Lead sorption by waste biomass of hazelnut and almond shell, J. Hazard. Mater. 167 (1–3) (2009) 1203–1208.
[57] M. Ahmed, F. Mashkoor, A. Nasar, Development, characterization, and utilization of magnetized orange peel waste as a novel adsorbent for the confiscation of crystal violet dye from aqueous solution, Groundw. Sustain. Dev. 10 (2020) 100322.
[58] J.I. Morán, V.A. Alvarez, V.P. Cyras, A. Vázquez, Extraction of cellulose and preparation of nanocellulose from sisal fibers, Cellulose 15 (2008) 149–159.
[59] X. Zhou, L.J. Broadbelt, R. Vinu, Chapter two - mechanistic understanding of thermochemical conversion of polymers and lignocellulosic biomass, Adv. Chem. Eng. 49 (2016) 95–198.
[60] B. Molinuevo-Salces, C. González-Fernández, X. Gómez, M. García-González, A. Morán, Vegetable processing wastes addition to improve swine manure anaerobic digestion: evaluation in terms of methane yield and SEM characterization, Appl. Energy 91 (1) (2012) 36–42.
[61] A. Khan, X. Wang, K. Gul, F. Khuda, Z. Aly, A. Elseman, Microwave-assisted spent black tea leaves as cost-effective and powerful green adsorbent for the efficient removal of Eriochrome black T from aqueous solutions, Egypt J Basic Appl Sci 5 (2) (2018) 171–182.
[62] O. Kalfa, Ö. Yalçınkaya, A. Türker, Synthesis of nano B2O3/TiO2 composite material as a new solid phase extractor and its application to preconcentration and separation of cadmium, J. Hazard. Mater. 166 (1) (2009) 455–461.
[63] S. Gubin, Y. Koksharov, G. Khomutov, G. Yurkov, Magnetic nanoparticles: preparation, structure and properties, Russ. Chem. Rev. 74 (6) (2005) 489–520.
[64] V. Le, V. Doan, T. Le, M. Dao, T. Vo, H. Do, et al., Efficient photocatalytic degradation of crystal violet under natural sunlight using Fe_3O_4/ZnO nanoparticles embedded carboxylate-rich carbon, Mater. Lett. 283 (2020), 128749.
[65] S. Gopi, A. Pius, S. Thomas, Enhanced adsorption of crystal violet by synthesized and characterized chitin nano whiskers from shrimp shell, J Water Process Eng 14 (2016) 1–8.
[66] A. Dabagh, A. Bagui, M. Abali, R. Aziam, M. Chiban, F. Sinan, M. Zerbet, Adsorption of crystal violet from aqueous solution onto eco-friendly native *Carpobrotus edulis* plant, Materials Today: Proceedings 37 (3) (2020) 3980–3986.
[67] Y. Bulut, Z. Tez, Adsorption studies on ground shells of hazelnut and almond, J. Hazard. Mater. 149 (1) (2007) 35–41.
[68] K. Ghosh, N. Bar, A.B. Biswas, S.K. Das, Elimination of crystal violet from synthetic medium by adsorption using unmodified and acid-modified eucalyptus leaves with MPR and GA application, Sustain. Chem. Pharm. 19 (2021) 100370.
[69] A. Krasilin Andrei, P. Danilovich Dmitry, B. Yudina Elena, Bruyere Stéphanie, Ghanbaja Jaafar, K. Ivanov Vladimir, Crystal violet adsorption by oppositely twisted heat-treated halloysite and pecoraite nanoscrolls, Appl. Clay Sci. 173 (2019) 1–11.
[70] R. El Haouti, H. Ouachtak, A. El Guerdaoui, A. Amedlous, E. Amaterz, R. Haounati, M.L. Taha, Cationic dyes adsorption by Na-montmorillonite nano clay: experimental study combined with a theoretical investigation using DFT-based descriptors and molecular dynamics simulations, J. Mol. Liq. 290 (2019), 111139.
[71] A.H. Tayeb, E. Amini, S. Ghasemi, M. Tajvidi, Cellulose nanomaterials—binding properties and applications: a review, Molecules 23 (10) (2018) 2684.
[72] P. Druzian Susanne, P. Zanatta Natalia, K. Borchardt Renata, N. Côrtes Letícia, F. M. Streit Angélica, C. Severo Eric, O. Gonçalves Janaína, L. Foletto Edson, C. Lima Eder, L. Dotto Guilherme, Chitin-psyllium based aerogel for the efficient removal of crystal violet from aqueous solutions, Int. J. Biol. Macromol. 179 (2021) 366–376.
[73] Zhao Xu, Qian Wen, Zhang Menghua, Li Zijian, Zhang Qinghua, Yang Zhijian, Dye-assembled two-dimensional porous HMX for enhanced energy release and safety performance, Energetic Materials Frontiers in press. 2 (2) (2021) 139–146.
[74] G. Derafa, H. Zaghouane-Boudiaf, Urtica dioica leaves-calcium alginate as a natural, low cost and very effective bioadsorbent beads in elimination of dyes from aqueous medium: equilibrium isotherms and thermodynamic studies, Int. J. Biol. Macromol. 124 (2019) 915–921.
[75] A.K. Sharma, B.S. Priya Kaith, J.K. Bhatia, S. Panchal, N. Sharma, V. Tanwar, Efficient capture of eosin yellow and crystal violet with high performance xanthan-acacia hybrid super-adsorbent optimized using response surface methodology, Colloid Surf Biointerface 175 (2019) 314–323.
[76] F.B. Scheufele, N. Módenes A, C.E. Borba, C. Ribeiro, R. Espinoza-Quiñones F, R. Bergamasco, N.C. Pereira, Monolayer–multilayer adsorption phenomenological model: kinetics, equilibrium and thermodynamics, Chem. Eng. J. 284 (2016) 1328–1341.
[77] C. Araújo, I. Almeida, H. Rezende, S. Marcionilio, J. Léon, T. de Matos, Elucidation of mechanism involved in adsorption of Pb(II) onto lobeira fruit (*Solanum lycocarpum*) using Langmuir, Freundlich and Temkin isotherms, Microchem. J. 137 (2018) 348–354.
[78] A. Mirza, R. Ahmad, An efficient sequestration of toxic crystal violet dye from aqueous solution by alginate/pectin nanocomposite: A novel and ecofriendly adsorbent, Groundw. Sustain. Dev. 11 (2020) 100373.
[79] J. Putro, S. Santoso, F. Soetaredjo, S. Ismadji, Y. Ju, Nanocrystalline cellulose from waste paper: adsorbent for azo dyes removal, Environ Nanotechnol Monitor Manage 12 (2019) 100260.
[80] J. Piccin, T. Cadaval, L. de Pinto, G. Dotto, Adsorption isotherms in liquid phase: experimental, modeling, and interpretations, in: Adsorption Processes For Water Treatment And Purification, 2017, pp. 19–51.
[81] Y.-Z. Wen, Y.-Q. Xue, Z.-X. Cui, Y. Wang, Thermodynamics of nanoadsorption from solution: theoretical and experimental research, J. Chem. Thermodynamics 80 (2015) 112–118.
[82] R.T. Tung. http://academic.brooklyn.cuny.edu/physics/tung/CULP/liquid2.htm.
[83] M.T. Yagub, T.K. Sen, S. Afroze, H.M. Ang, Dye and its removal from aqueous solution by adsorption: a review, Adv. Colloid Interf. Sci. 209 (2014) 172–184.